

RESEARCH ARTICLE

10.1002/2015JD024292

Key Points:

- A fuel-based inventory for NO_x and CO in the Los Angeles Basin was developed
- The inventory was evaluated with the CalNex in situ and remote sensing data
- A regional model using this inventory reproduced observed weekly cycle of emissions and chemistry

Supporting Information:

- Figures S1–S13 and Tables S1–S6

Correspondence to:

S.-W. Kim,
siwan.kim@noaa.gov

Citation:

Kim, S.-W., et al. (2016), Modeling the weekly cycle of NO_x and CO emissions and their impacts on O₃ in the Los Angeles-South Coast Air Basin during the CalNex 2010 field campaign, *J. Geophys. Res. Atmos.*, 121, 1340–1360, doi:10.1002/2015JD024292.

Received 30 SEP 2015

Accepted 6 JAN 2016

Accepted article online 10 JAN 2016

Published online 12 FEB 2016

Modeling the weekly cycle of NO_x and CO emissions and their impacts on O₃ in the Los Angeles-South Coast Air Basin during the CalNex 2010 field campaign

S.-W. Kim^{1,2}, B. C. McDonald^{1,2,3}, S. Baidar^{2,4}, S. S. Brown¹, B. Dube^{1,2}, R. A. Ferrare⁵, G. J. Frost¹, R. A. Harley³, J. S. Holloway^{1,2}, H.-J. Lee^{1,2}, S. A. McKeen^{1,2}, J. A. Neuman^{1,2}, J. B. Nowak^{1,2,6}, H. Oetjen⁴, I. Ortega⁴, I. B. Pollack^{1,2,7}, J. M. Roberts¹, T. B. Ryerson¹, A. J. Scarino⁵, C. J. Senff^{1,2}, R. Thalman^{2,4}, M. Trainer¹, R. Volkamer^{2,4}, N. Wagner^{1,2}, R. A. Washenfelder^{1,2}, E. Waxman^{2,4}, and C. J. Young^{1,2,8}

¹Chemical Sciences Division, NOAA Earth System Research Laboratory, Boulder, Colorado, USA, ²Cooperative Institute for Research in Environmental Sciences, University of Colorado Boulder, Boulder, Colorado, USA, ³Department of Civil and Environmental Engineering, University of California, Berkeley, California, USA, ⁴Department of Chemistry and Biochemistry, University of Colorado Boulder, Boulder, Colorado, USA, ⁵NASA Langley Research Center, Hampton, Virginia, USA, ⁶Now at Aerodyne Research, Inc., Billerica, Massachusetts, USA, ⁷Now at Department of Atmospheric Science and Department of Chemistry, Colorado State University, Fort Collins, Colorado, USA, ⁸Now at Department of Chemistry, Memorial University, St. John's, Newfoundland and Labrador, Canada

Abstract We developed a new nitrogen oxide (NO_x) and carbon monoxide (CO) emission inventory for the Los Angeles-South Coast Air Basin (SoCAB) expanding the Fuel-based Inventory for motor-Vehicle Emissions and applied it in regional chemical transport modeling focused on the California Nexus of Air Quality and Climate Change (CalNex) 2010 field campaign. The weekday NO_x emission over the SoCAB in 2010 is 620 t d⁻¹, while the weekend emission is 410 t d⁻¹. The NO_x emission decrease on weekends is caused by reduced diesel truck activities. Weekday and weekend CO emissions over this region are similar: 2340 and 2180 t d⁻¹, respectively. Previous studies reported large discrepancies between the airborne observations of NO_x and CO mixing ratios and the model simulations for CalNex based on the available bottom-up emission inventories. Utilizing the newly developed emission inventory in this study, the simulated NO_x and CO mixing ratios agree with the observations from the airborne and the ground-based in situ and remote sensing instruments during the field study. The simulations also reproduce the weekly cycles of these chemical species. Both the observations and the model simulations indicate that decreased NO_x on weekends leads to enhanced photochemistry and increase of O₃ and O_x (=O₃ + NO₂) in the basin. The emission inventory developed in this study can be extended to different years and other urban regions in the U.S. to study the long-term trends in O₃ and its precursors with regional chemical transport models.

1. Introduction

California has a long history of severe air quality problems because of its large urban population and unique meteorological and geographic conditions favorable to heavy smog formation [Haagen-Smit, 1952; Lawson, 1990; Jacobson et al., 1996; Lu et al., 1997; Marr and Harley, 2002; Fujita et al., 2003; Harley et al., 2005; Jacobson, 2005; Ryerson et al., 2013]. The South Coast Air Basin (SoCAB) encompasses the urban areas of Los Angeles (LA), Orange, Riverside, and San Bernardino counties in Southern California. The SoCAB had a population of over 17 million inhabitants in 2010 (factfinder.census.gov) and is surrounded by mountainous terrain, and the Pacific Ocean. Large urban pollution from the SoCAB is often trapped in the basin [Lu and Turco, 1994] and has the ability to increase to a critical level that can cause damage to human health and ecosystems. In addition, several studies have reported that O₃ and its precursors are transported from the SoCAB to other western states and affect O₃ levels in these regions [White et al., 1990; Langford et al., 2010; Huang et al., 2013]. For the last half-century, there have been extensive efforts to reduce emissions and pollution in the SoCAB. Recent studies of California air quality reported much cleaner air in 2010 compared to the 1960s and 1970s: ambient carbon monoxide (CO), sulfur dioxide (SO₂), nitrogen oxides (NO_x = NO + NO₂), volatile organic compounds (VOCs), and O₃ have been reduced because of air pollution controls and despite a large increase in population over the same period [McDonald et al., 2012, 2013; Russell et al., 2012; Warneke et al., 2012; Pollack et al., 2013]. Regional chemical transport modeling of the long-term trend of O₃ and its precursors in the SoCAB may provide comprehensive knowledge of the evolving chemistry and transport

within the basin and beyond, as well as improved understanding of the effectiveness of air pollution controls in the past and the future. Intensive field data are critical for validating various aspects of state-of-the-art chemical transport models, including the emission inventories that are fundamental inputs to such models. The California Nexus of Air Quality and Climate Change (CalNex) intensive field campaign that occurred in May–July 2010 measured atmospheric trace gases from airborne, ship, and ground-based platforms to better understand the emissions of ozone precursors and greenhouse gases in California [Ryerson *et al.*, 2013]. During this field study, there were extensive measurements of NO_x and CO mixing ratios on various platforms that provide a basis for evaluating the emission inventories and investigating urban chemistry.

In urban regions, NO_x is released into the troposphere mainly as a result of anthropogenic activity and plays an important role in tropospheric chemistry as a major precursor of ozone and aerosols. CO is emitted from anthropogenic sources as well as natural sources, such as wildfires, and is a precursor of O_3 and is also produced from VOC oxidation. In addition, CO emissions are often used as a tracer for emissions of other species, including VOCs. For example, the CO to carbon dioxide (CO_2) ratio and the VOC to CO ratio can be used to validate emission inventories [Borbon *et al.*, 2013; Brioude *et al.*, 2013; Pollack *et al.*, 2012, 2013; Warneke *et al.*, 2012, 2013]. Thus, developing accurate NO_x and CO emission estimates is a critical step in understanding past, present, and future air quality in California. The objectives of this study are to develop bottom-up NO_x and CO emission inventories to support air quality modeling in the SoCAB during CalNex and to evaluate the emission inventory and related chemistry using field measurements and regional model simulations. This method is also appropriate for improving mobile source emission inventories in other regions of the U.S.

2. Development of Emission Inventory

In the SoCAB, McDonald *et al.* [2012, 2013] report a fuel-based estimate of CO_2 , CO, NO_x , and VOC emissions from on-road engines, using taxable fuel sales and roadway measured emission factors for gasoline- and diesel-powered motor vehicles. In addition, McDonald *et al.* [2014] developed high-resolution maps of on-road CO_2 emissions over several urban regions in the U.S. The new emission inventory is referred to the Fuel-based Inventory for motor Vehicle Emission (FIVE). A notable feature of FIVE is the separate spatial and temporal mapping of on-road gasoline and diesel emissions, utilizing highway traffic count, weigh-in-motion, and fuel sales data that distinguish between the two classes of engines. For example, in FIVE, higher fractions of diesel traffic are found near major freight facilities and away from urban cores. Also, large decreases in diesel engine activity on weekends relative to weekdays are taken into account, as well as separate diurnal profiles for gasoline and diesel engines that vary between weekdays and weekends.

In this study, we expand FIVE to include CO and NO_x emissions in addition to CO_2 . CO_2 emissions are first mapped at $4 \text{ km} \times 4 \text{ km}$ horizontal resolution across the state of California. CO and NO_x emissions are then scaled from maps of CO_2 with emission factors normalized to fuel use from McDonald *et al.* [2012, 2013]. This scaling is performed separately for on-road gasoline and diesel engines. Excess emissions from gasoline engine starting are included from California's EMFAC2011 model (<http://www.arb.ca.gov/emfac/2011/>).

In addition to on-road emissions, off-road, areawide, and stationary sources are included in the inventory for the model simulations as shown in Table 1. For these source categories, emissions are either calculated by a fuel-based approach or adopted from the California Air Resources Board (CARB) 2009 Almanac projection to 2010 (<http://www.arb.ca.gov/app/emsinv/fcemssumcat2009.php>) and allocated to the model grid following the spatial and temporal distributions in the U.S. Environmental Protection Agency (EPA) National Emission Inventory for 2005 (NEI05; see Kim *et al.* [2011] for more information). NEI05 was the most up-to-date EPA emission inventory until 2011 when the NEI08 was released and has been extensively used to support atmospheric chemistry and transport modeling of the LA Basin [Chen *et al.*, 2013; Brioude *et al.*, 2013; Huang *et al.*, 2014]. In this study, NEI05 was used only for temporal and spatial allocations for specific sectors, while the total emission estimates for these sectors are independent of the NEI05. More information on the emission inventory developed in this study that includes diurnal and weekly cycles and spatial distributions is given in Figures S1–S4 in the supporting information.

Table 1. NO_x Emissions (NO₂ Metric Tons per Day) in the SoCAB During Ozone Season Weekdays^a

Sources or Emission Inventories	NEI05	NEI11	This Study (2010)
All sources ^b	890	660	620
On-road mobile sources	480	480	470
- Gasoline-powered vehicle	290	180	230
- Diesel-powered vehicle	190	300	240
Other mobile sources ^b	270	88	81
- Off-road equipment	120	59	50 ^c
- Commercial marine vessel	105 ^d	5 ^d	4
- Locomotive	40 ^d	20 ^d	24
- Farm equipment	0.7 ^d	4 ^d	3
Areawide and stationary sources	140 ^e	91 ^e	72 ^f

^aThe emissions developed in this study that represent 2010 are compared to those in NEI05 and NEI11. Here the boundary of the SoCAB defined by CARB is used.

^bFor other mobile sources, only diesel engine emissions are included. Therefore, the NEI05 and NEI11 emissions in this table correspond to 94% and 96% of NEI05 and NEI11 of all anthropogenic sources emissions, respectively.

^cFuel-based estimate of off-road diesel equipment from *McDonald et al.* [2012]. The emission from this sector projected to 2010 in the CARB 2009 Almanac-Standard Emissions Tool is 161.0 (t d⁻¹), which is 3 times higher than the estimation in this study for 2010.

^dCommercial marine vessels, locomotive, and farm equipment are included in the area source category in the NEI05.

^eNEI05 point and area source emissions are merged. Excluded from the area sources here are commercial marine vessel, locomotive, farm equipment, and residential heating and cooling.

^fEmissions are from the CARB 2009 Almanac-Standard Emissions Tool.

In the SoCAB, other mobile source emissions of NO_x are primarily from off-road diesel equipment (e.g., for construction, industrial, commercial, and military purposes), commercial marine vessels (e.g., harbor craft and oceangoing vessels), and locomotives, with small fractions from farm equipment in the eastern portion of the basin (Table 1). The fuel-based approach is used to estimate NO_x emissions for these sectors, following *Kean et al.* [2003], *Dallmann and Harley* [2010], and *McDonald et al.* [2012]. Off-road diesel fuel consumption by end-use category is reported for each state by the *Energy Information Administration (EIA)* [2012]. NO_x emission factors for off-road diesel equipment, marine vessels, and locomotives are from *Dallmann and Harley* [2010] and updated to 2010 by *McDonald et al.* [2012]. NO_x emissions are calculated as the product of off-road fuel use and NO_x emission factors,

and spatially apportioned from the state to air basin level using the CARB 2009 Almanac. For marine vessels operating within SoCAB, we only include emissions from the combustion of diesel fuel and exclude emissions from marine residual fuel oil. Since 2009, California has mandated that oceangoing vessels that operate within 24 nautical miles of the coast switch to cleaner burning diesel fuel.

VOC emission estimates are also required to simulate day-of-week O₃ cycles with a regional chemical transport model. In this study, we rely on NEI05 estimates of VOC emissions. Previous studies reported that the weekday-to-weekend O₃ changes in the LA Basin were mainly caused by NO_x emission changes [*Warneke et al.*, 2013; *Yarwood et al.*, 2008].

3. Regional Chemical Transport Model

In this study, the regional chemical transport model serves as a transfer standard for connecting emissions to atmospheric chemical observations because the model accounts for transport and chemistry. We use version 3.4.1 of the Weather Research and Forecasting-Chemistry model (WRF-Chem) [*Grell et al.*, 2005]. The mother and the nested domains of the WRF-Chem model are the western U.S. (12 km × 12 km horizontal resolution) and the state of California (4 km × 4 km horizontal resolution), respectively. The model has 60 vertical levels with ~50 m thickness between vertical levels up to 4 km aboveground level, with coarser vertical resolution at higher levels. The first model level where mixing ratios of chemical species are calculated is ~25 m. The WRF-Chem diagnoses surface wind vector and temperature at 10 m and 2 m aboveground level, respectively, for comparison with the observations from the surface meteorology stations. The simulation period is 26 April 2010 to 17 July 2010. Meteorological initial and boundary conditions are based on National Centers for Environmental Prediction Global Forecast System data. The MOZART (Model for OZone and Related chemical Tracers, <http://www.acom.ucar.edu/wrf-chem/mozart.shtml>) [*Emmons et al.*, 2010] global model results are used as initial and boundary conditions for the mother domain of WRF-Chem. Biogenic emissions are based on the Biogenic Emissions Inventory System version 3.13, and emissions from urban vegetation [*Scott and Benjamin*, 2003] are added. The Noah land surface model, Yonsei University (YSU) planetary boundary layer model, Lin microphysics scheme, and Grell-Devenyi ensemble cumulus parameterization (only for the mother domain) are adopted (see references in *Kim et al.* [2009]). The chemical mechanism is based on the Regional

Atmospheric Chemistry Mechanism [Stockwell *et al.*, 1997] with ~30 reaction rate coefficients updated [Kim *et al.*, 2009]. The model-simulated meteorology agrees with the observations from the surface stations and by aircraft. Refer to Figures S5–S9 and Table S1 in the supporting information for details including comparison with the planetary boundary layer (PBL) heights from aerosol lidar [Hair *et al.*, 2008; Alvarez *et al.*, 2011; Scarino *et al.*, 2014]. Angevine *et al.* [2012] reported performance of the WRF model for CalNex with other physical options. Since the transport model reasonably represents the meteorology in the SoCAB, differences between model and observations are attributed to emissions and chemistry, as discussed in section 5.

4. Observational Data Sets

4.1. The CalNex Field Campaign Data

4.1.1. In Situ Observations

4.1.1.1. Airborne Measurement of CO, NO, NO₂, PAN, HNO₃, and O₃ on P-3

We utilize airborne measurements of trace gases made during seven daytime flights (4, 8, 14, 16, 19, 24 May and 20 June). During these times, the NOAA P-3 aircraft made extensive measurements mainly in the PBL and in the eastern part of the SoCAB where both local and upwind (LA urban core) sources affect ambient levels of trace gases. Four weekday and three weekend flights are used to examine the dependence of emissions and chemistry on the day-of-week cycle. CO was measured by vacuum UV resonance fluorescence [Holloway *et al.*, 2000]. NO_x species and O₃ were provided by either chemiluminescence [Ryerson *et al.*, 1999; Ryerson *et al.*, 2000; Pollack *et al.*, 2011] or cavity ring-down spectroscopy [Wagner *et al.*, 2011]. Peroxyacetyl nitrates (PAN) [Slusher *et al.*, 2004; Roiger *et al.*, 2011] and HNO₃ [Neuman *et al.*, 2002, 2003] were measured by chemical ionization mass spectrometry. The time resolution is 1 s for most species (2 s for PAN), and corresponding horizontal spatial resolution is ~100 m. Accuracies of NO_x, O₃, and CO measurements are less than or equal to 5%, while accuracies of HNO₃, PAN, and NH₃ are 15%, 20%, and 30%, respectively. The air masses with the NH₃ mixing ratio <10 ppbv are selected for analysis of HNO₃, PAN, and NO_y (=NO_x + PAN + HNO₃) to avoid interferences with NH₃ following Pollack *et al.* [2012]. More details on instruments and references are given in Ryerson *et al.* [2013]. The P-3 data representing boundary layer conditions (collected below ~1 km aboveground level) have been averaged at the model spatial resolution (4 km) to allow one-to-one comparison of the observations and model results.

4.1.1.2. Ground-Based NO₂ and CO Observations in Pasadena

NO₂ and CO mixing ratios observed at the ground site in Pasadena during May and June 2010 are compared with the model simulations. NO₂ was measured using cavity ring-down spectroscopy (CRDS) [Washenfelder *et al.*, 2011] and cavity enhanced differential optical absorption spectroscopy (CE-DOAS) [Thalman and Volkamer, 2010], and CO was provided by vacuum UV fluorescence [Gerbig *et al.*, 1999]. The CE-DOAS instrument was located on the Caltech Milliken library roof. The time resolution of the measurements is 1 min. The data have been averaged for 1 h prior to the comparison with the model results.

4.1.2. Remote Sensing Data

4.1.2.1. CU-AMAX-DOAS NO₂ Column on NOAA Twin Otter

The University of Colorado Airborne Multi-Axis Differential Optical Absorption Spectroscopy (CU AMAX-DOAS) instrument was deployed aboard the NOAA Twin-Otter during May–July 2010 and provides the spatial and temporal distributions of NO₂ columns below the aircraft altitude (~4 km). The instrument design, resolution, retrieval algorithm, and accuracy have been characterized [Baidar *et al.*, 2013a] and have been compared with in situ and lidar measurements [Volkamer *et al.*, 2015]. Analysis of the DOAS measurements gives the integrated concentration of trace gases along the light path relative to a reference spectrum (zenith in this case), referred to the NO₂ differential slant column density. The nadir differential slant column from the AMAX-DOAS was converted to a tropospheric vertical column by applying the geometric air mass factor correction. A sensitivity study using the McArtim radiative transfer model (RTM) [Deutschmann *et al.*, 2011] revealed that the geometric approximation is a viable option to convert nadir NO₂ slant columns to vertical columns, with errors <~7%, for solar zenith angle <65°, and smaller retrieval errors under smaller solar zenith angles [Baidar *et al.*, 2013a]. The CU AMAX-DOAS instrument is validated by comparison with NO₂ columns measured by a ground-based MAX-DOAS [Baidar *et al.*, 2013a]. Furthermore, reasonable agreement was reported between the CU-AMAX-DOAS and satellite NO₂ column data [Oetjen *et al.*, 2013], and the NO_x emission inventory for Bakersfield, CA [Baidar *et al.*, 2013b]. We utilized the AMAX-DOAS data from a total of eight flights (five weekday and three weekend flights) covering the SoCAB during May–July 2010. The selected flights

provide data under solar zenith angles $< \sim 30^\circ$ and have minimal retrieval errors. These flights were made in both the western and eastern parts of the basin and between morning and early afternoon. The horizontal resolution of the measurements is about 1 km. For comparing AMAX-DOAS data to model simulations, the AMAX-DOAS data have been averaged at the model spatial resolution (4 km) and the model columns are integrated from the surface to the Twin-Otter flight altitude.

4.1.2.2. Ground-Based CU-MAX-DOAS Observations of NO₂ Columns

The measurements from the ground-based University of Colorado (CU) MAX-DOAS [Coburn *et al.*, 2011] during the CalNex intensive period were carried out in Pasadena, CA, on the roof of Caltech Milliken library. The period of measurement was May–November 2010. In this study, we utilized the NO₂ column retrieval data covering May–July 2010 when the model simulations are available. NO₂ differential slant columns were converted to vertical columns using the geometric air mass factor with a 10° elevation angle, which shows better agreement with results carried out with RTM calculations and suffers less from relative azimuth angle dependencies (A. Richter, personal communication, 2015). During CalNex, the view direction of the instrument was west-east in order to capture possible gradients. In order to identify and filter cloudy periods, the ratio of radiances at two different wavelengths, in this case 350 to 450 nm, is used [Wagner *et al.*, 2014]. Based on sensitivity studies and by inspection, a ratio greater than 0.23 identifies cloud-free days. The time resolution of the measurements is ~ 13 min. The data have been averaged for 1 h prior to the comparison with the model results, which have also been averaged for 24 km to match the approximate horizontal spatial scale probed by the MAX-DOAS instrument.

4.2. The AQMD Surface Monitoring Data

The hourly NO_x, CO, and O₃ data from the South Coast Air Quality Management District (AQMD) monitoring network (<http://www.arb.ca.gov/aqmis2/aqdselect.php>) for 21 sites are utilized to evaluate the emission inventories. The locations of the sites and the data are shown in Table S2 and Figures S10 and S11. Details on standard procedures for maintaining and operating air monitoring stations and specific instrumentations are provided in the CARB air monitoring Web manual (<http://www.arb.ca.gov/airwebmanual/index.php>). AQMD uses chemiluminescence detection with a Molybdenum converter to measure surface NO₂. Other oxygenated nitrogen species are known to contribute to the NO₂ measured by this method [Fehsenfeld *et al.*, 1987; Dunlea *et al.*, 2007]. However, contributions of the oxygenated nitrogen species to the measured NO₂ are not well quantified. This depends on inlet configuration and thermal operation range of a molybdenum converter [Pollack *et al.*, 2013]. The ratios of PAN, HNO₃, and organic nitrates to measured NO₂ can differ from one location to another. Although the AQMD measurements may not be as accurate as the field measurements obtained during CalNex, these routine monitor data are available for many decades and can serve as a comparison standard for air quality modeling research that examines long-term trends.

5. Results and Discussion

5.1. Emission Inventory

Table 1 compares weekday sectorial NO_x emissions from the NEI05, NEI11, and this study in the SoCAB. Refer to Ahmadov *et al.* [2015] for discussion of the NEI11 data set. Total NO_x emissions are 620 t d⁻¹ in this study, 30% less than NEI05. This study's total NO_x emissions are similar to total NO_x emissions in the NEI11, 660 t d⁻¹. Several studies [Chen *et al.*, 2013; Brioude *et al.*, 2013; Huang *et al.*, 2014] have pointed out that the model simulation of NO_x mixing ratios using NEI05 emissions overestimated NO_x during CalNex. The NO_x emissions from on-road engines in this study and NEI05 are similar, while emissions from other source categories in this study are 60% lower than in the NEI05. In the NEI05, on-road sources account for 54% of total NO_x emissions, versus 75% of total NO_x emissions in this study. Therefore, on-road emissions dominate NO_x in the SoCAB in this study. The on-road NO_x emissions and ratio of those to total emissions in this study and NEI11 are similar. However, NEI11 estimates higher on-road diesel NO_x emissions and less on-road gasoline-engine emissions than this study.

The differences between the NEI05 and NEI11 data sets not only highlight the importance of using updated emission inventories in air quality model simulations but also reveal important changes in methodology that occurred. For example, on-road emissions are unchanged between the NEI05 and NEI11 (Table 1), inconsistent with emission control policies implemented on light- and heavy-duty vehicles [McDonald *et al.*, 2012] (see also Table 2 in this manuscript). This may be explained by the different emission models used in the two different years of the NEI. On-road emissions for California in the NEI05 [Environmental Protection Agency (EPA), 2008]

Table 2. NO_x Emissions (NO₂ Metric Tons per Day) Changes Between 2005 and 2010 in the SoCAB in the Expanded FIVE Developed in This Study^a

Sources or Emission Year	2005	2010
All sources ^b	920	620
On-road mobile sources	730	470
- Gasoline-powered vehicle	390	230
- Diesel-powered vehicle	340	240
Other mobile, areawide, and stationary sources	185	153

^aThe emissions for ozone season weekdays are shown. Here the boundary for the SoCAB defined by CARB is used.

^bFor other mobile sources, only diesel engine emissions are included.

and NEI11 [EPA, 2015] were estimated using EPA's MOBILE6 and CARB's EMFAC models, respectively. Because California submitted on-road emissions for the NEI11 using CARB's emission models, the comparison of NO_x emissions between this study and the NEI11 may only be valid in California. Mobile source emissions in other states are estimated using EPA's Motor Vehicle Emission Simulator model (<http://www3.epa.gov/otaq/models/moves/>) in the NEI11. Anderson *et al.* [2014] report that the NEI11 overpredicts mobile source emissions of NO_x by 51–70% as compared to observations made in Maryland during the DISCOVER-AQ campaign (<http://science.nasa.gov/missions/discover-aq/>).

NO_x emissions from off-road diesel equipment and commercial marine vessels drive the differences in other mobile source emissions in the NEI05 and this study: off-road diesel equipment and commercial marine vessel emissions are 58% and 96% lower in this study than their NEI05 counterparts, respectively. Off-road emissions in the NEI05 were estimated using EPA's NONROAD model [EPA, 2008]. By contrast, off-road NO_x emissions in the NEI11 agree with estimates in this study and are from CARB's OFFROAD model [EPA, 2015]. The large differences in the NEI05 and NEI11 cannot be explained by reduced off-road activity expected from the Great Recession of 2008. Off-road diesel fuel use increased by 40% between 2005 and 2010, and diesel fuel use in marine vessels decreased by 33% [EIA, 2012]. For comparison, a fuel-based estimate of off-road emissions is shown in Table 1 and accounts for trends in emission factors and activity. In this study, NO_x emission factors of diesel equipment are based on EPA's NONROAD model [Dallmann and Harley, 2010; McDonald *et al.*, 2012], which are similar to CARB's OFFROAD model (<http://www.arb.ca.gov/msei/categories.htm>). We deduce that the discrepancy between the NEI05 and this study is mostly due to estimates of off-road activity, which appear to have been revised by CARB in the NEI11. In the past, potentially large errors in CARB estimates of NO_x emissions from off-road construction equipment were reported by Millstein and Harley [2009]. Utilizing their model simulations of Houston, Texas, Kim *et al.* [2011] demonstrated overestimation of NO_x emissions from commercial marine vessels in the NEI05, potentially due to errors in fuel types, emission factors, and spatial allocations. California started the implementation of several pollution regulations on commercial marine vessels operated by diesel fuel engines, such as switching to alternative fuels within 24 nautical miles from ports, and a vessel speed reduction program before 2010 (<http://www.arb.ca.gov/ports/marinevess/marinevess.htm>). NO_x emissions from areawide and stationary sources from the CARB 2009 Almanac are 50% of the NEI05 values.

Several studies [Russell *et al.*, 2012; Hilboll *et al.*, 2013; Pollack *et al.*, 2013] have suggested that ambient levels of NO_x or the sum of reactive nitrogen species (NO_y) in the SoCAB has declined in past decades, and reduction in on-road motor vehicle emissions is a main driver for this trend [Ban-Weiss *et al.*, 2008a, 2008b; Bishop and Stedman, 2008; McDonald *et al.*, 2012]. However, the analysis of bottom-up emission inventories (Table 1) indicates major methodological changes in the NEI that complicate model-based evaluations of long-term air quality and emission trends. An advantage of the fuel-based inventory used in this study for mobile source emissions is that a consistent methodology can be extended over long time periods (Table 2) [McDonald *et al.*, 2012; McDonald *et al.*, 2013].

Table 3 compares the weekday CO emissions from the NEI05 and this study for the SoCAB. Total CO

Table 3. CO Emissions (Metric Tons per Day) in the SoCAB During Ozone Season Weekdays^a

Sources or Emission Inventories	NEI05	NEI11	This Study (2010)
All sources	6500	2300	2300
On-road mobile sources	2800	1500	1300
- Gasoline	2760	1410	1200
- Diesel	70	65	80
Other mobile sources	3500 ^b	710 ^b	880 ^c
Areawide and stationary sources	180	105	144 ^c

^aHere the boundary of the SoCAB defined by CARB is used.

^bEmissions from commercial marine vessel, locomotive, and farm equipment are included, but these account for only ~1% of other mobile sources emissions in the NEI05.

^cEmissions are from the CARB 2009 Almanac-Standard Emissions Tool.

Table 3 compares the weekday CO emissions from the NEI05 and this study for the SoCAB. Total CO

Table 4. The Weekday and Weekend NO_x and CO Emissions (Metric Tons per Day) Over the SoCAB in the Inverse Model [Brioude et al., 2013] and in This Study^a

Emission Inventory	Weekdays	Weekends
NO _x		
Inversion	600	360
This study		
- Total	620	410
- On-road only (gas./diesel)	470 (230/240)	290 (200/90)
CO		
Inversion	3900	3300
This study		
- Total	2300	2200
- On-road only (gas./diesel)	1300 (1200/80)	1150 (1120/30)

^aHere the boundary of the SoCAB defined by CARB is used.

emissions are 2300 t d⁻¹, which is 64% less than the NEI05. Emissions from gasoline engines dominate on-road CO emissions in both the NEI05 and FIVE (Table 3). On-road CO emissions in FIVE are 54% lower than the NEI05 counterpart. In the NEI05, other mobile source emissions, primarily from off-road gasoline engines, contribute 54% of total CO emissions and are about 4 times higher than estimates in the CARB 2009 Almanac-Standard Emissions Tool. Off-road emissions changed little between 2005 and 2010 according to CARB.

Therefore, differences between the NEI05 and CARB must be due to methodological differences in activity or emission factors. Off-road CO emissions in this study are 38% of total CO emissions over the SoCAB. Areawide and stationary source CO emissions are only small fractions (<6%) in 2010. As for NO_x, Chen et al. [2013] and Brioude et al. [2013] demonstrated overestimation of CO emissions in the NEI05 version in Table 3. Total and sectorial CO emissions in NEI11 and this study agree closely as shown in Table 3.

FIVE provides day of week specific on-road emissions for California. NO_x emissions for off-road diesel equipment and farm equipment on weekends are reduced by 72% and 50%, respectively, compared to weekdays as in Chinkin et al. [2003]. Weekday and weekend NO_x emissions are set to be the same for the other nonmobile source emissions. Table 4 summarizes weekday and weekend emissions, respectively. The emissions from the inverse model approach [Brioude et al., 2013] are included in the table for comparison. Our weekday and weekend estimates of NO_x emissions for the SoCAB are 620 and 410 t d⁻¹, respectively, showing a 34% reduction of NO_x on weekends compared to weekdays. Weekday-weekend differences in gasoline-powered vehicle NO_x emissions are small, while diesel-powered vehicle emissions on weekends are 62% lower than on weekdays due to reductions in heavy-duty truck traffic [Harley et al., 2005; McDonald et al., 2012]. Weekday and weekend NO_x emissions estimated by inverse modeling [Brioude et al., 2013] based on the P-3 NO_y observations during CalNex are 600 and 360 t d⁻¹, respectively, which are only 3% lower for weekdays and 12% lower for weekends than the estimates in this study.

Our weekday and weekend CO emissions are 2300 and 2200 t d⁻¹, respectively, which is only an ~5% reduction of CO on weekends compared to weekdays. As shown in Tables 3 and 4, gasoline-powered vehicle contributions dominate total on-road CO emissions. Small weekday-to-weekend changes in gasoline-powered vehicle activity cause relatively small day-of-week variation in CO emissions. The inverse model-based CO emissions also show small weekday-to-weekend changes: a 15% reduction on weekends compared to weekdays. However, the inverse model estimates are 50–70% higher than the total CO emissions estimated in this study (Table 4). To get a daily CO emission from the daytime inversion estimation, the NEI05 diurnal profile of CO emission is applied, following Brioude et al. [2013]. The diurnal profile of CO in NEI05 may not be accurate, considering the large overestimation in the NEI05 CO emissions from other mobile sources that do not change much through the day (Table 3). The inverse model estimations are only 30–50% higher than the CO emissions in this study when only daytime emissions (10–18 local time) are compared. In addition, 24 h backward trajectories for estimation of CO emission may not capture recirculation of this pollutant within the SoCAB. A sensitivity test using 72 h trajectories reduces the inversion-based CO emissions by ~10% (J. Brioude and Y. Cui, personal communications, 2015). Yan et al. [2014] confirmed that the relatively long lifetime of CO caused enhancements to be carried across the globe and affected background CO. They found that the simulated CO was quite sensitive to the spatial resolutions of the chemical transport model. Modeling CO is a challenging task, which in turn can affect an accuracy of inversion of CO emissions.

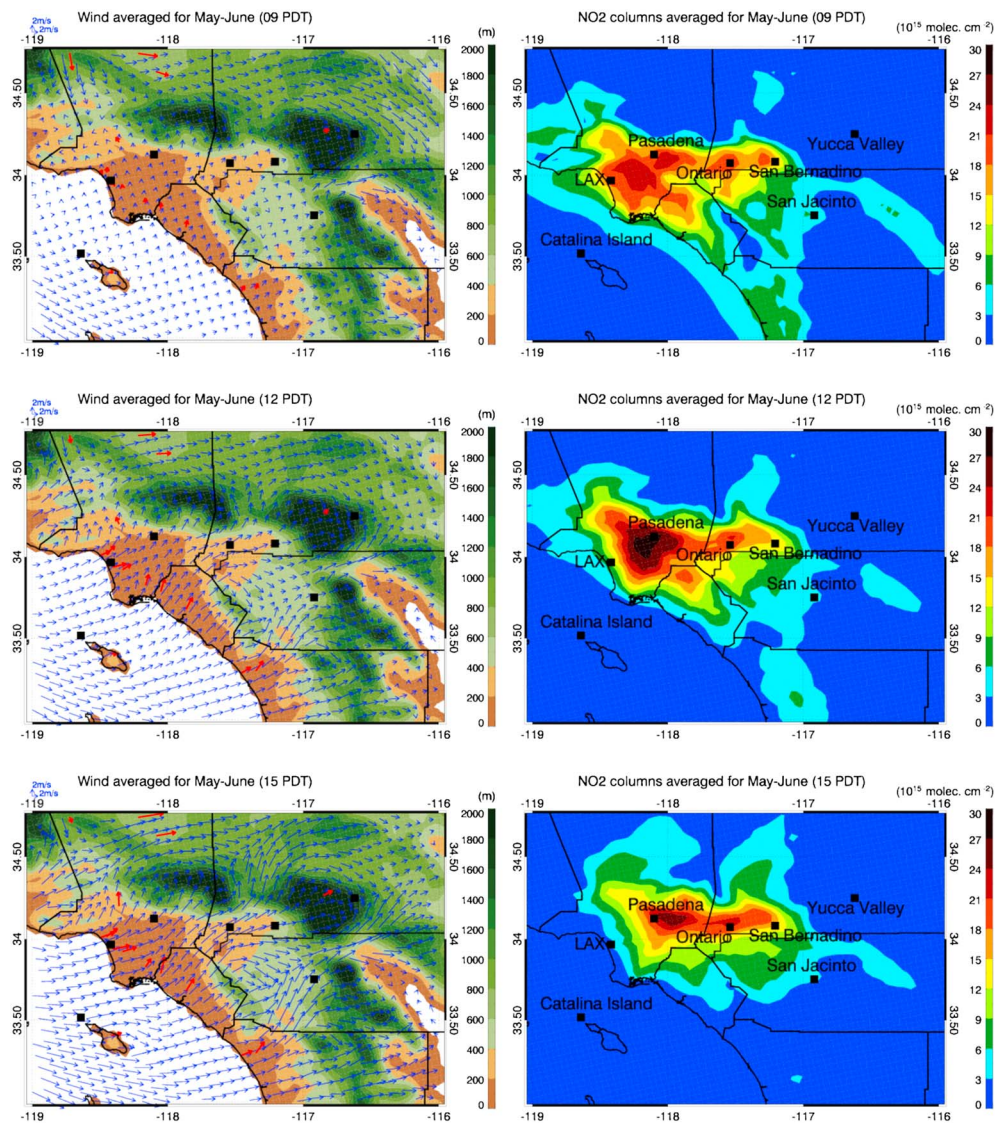


Figure 1. Spatial distributions of (left) the model surface wind and terrain height and (right) NO₂ columns in the SoCAB at (top) 09:00 PDT, (middle) 12:00 PDT, and (bottom) 15:00 PDT. The observed wind vectors at surface stations are included as red arrows.

5.2. Comparison of CalNex In Situ NO_x and CO Observations and Model Results

5.2.1. Aircraft Observations of NO_x and CO Over the SoCAB

The P-3 data were utilized to study total emissions and chemistry over the SoCAB [Pollack *et al.*, 2012, 2013; Warneke *et al.*, 2013]. Figure 1 shows the evolution of the simulated wind and NO₂ plumes within the SoCAB and characterizes the air masses that the P-3 aircraft sampled. Winds are calm in the basin in the early morning and then sea breezes develop from the morning to the afternoon. In the early morning, NO₂ columns represent fresh local emissions and residuals from nighttime with the largest plumes being located west of Pasadena. As sea breezes develop, the main plumes are transported east to the central basin, and the peak at noon is located near Pasadena. In the afternoon, the plumes move east of Pasadena. During CalNex, 90% of the SoCAB P-3 flights utilized in this study were made in the afternoon and 90% of the tracks of these afternoon flights were located east of Pasadena. Therefore, the P-3 flights sampled the air masses affected by the emissions across the broader basin.

An accurate transport model of vertical mixing directly affects the evaluation of emissions and chemistry using the P-3 data and regional model simulations. Sea-land contrasts, complex terrain, and inhomogeneous land use cause large spatial gradients of air temperature in the basin, which in turn influences the spatial

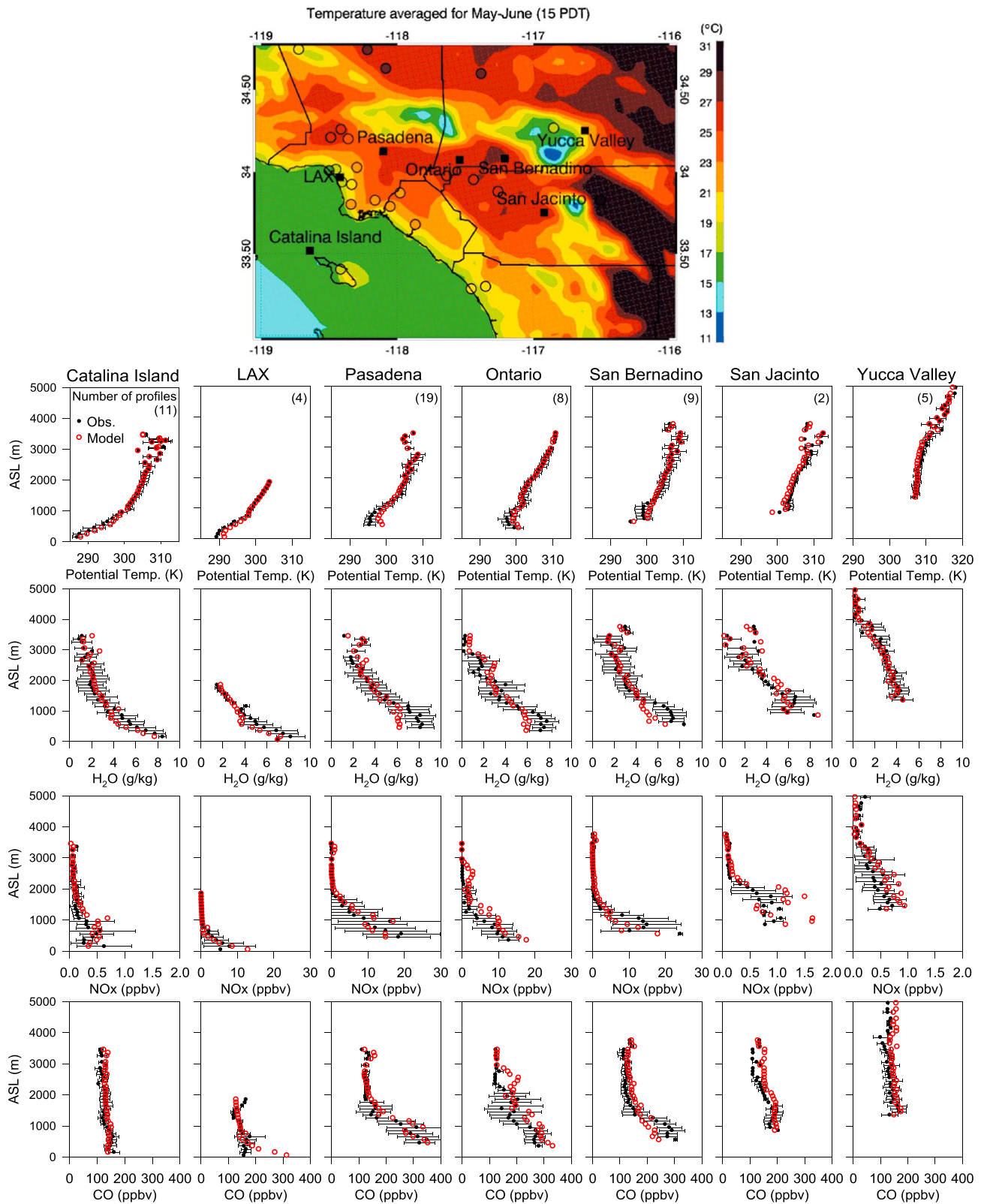


Figure 2. (top) Average May–June spatial distribution of temperature in the basin at 15:00 PDT and (bottom) averaged vertical profiles of the NOAA P-3 observed (black filled circles) and simulated (red open circles) potential temperature, water vapor, NO_x, and CO at Catalina Island, Los Angeles International Airport (LAX), Pasadena, Ontario, San Bernardino, San Jacinto, and Yucca Valley. The size of vertical bin is 100 m. Standard deviations of the observations are shown as error bars. The observed temperature at surface stations is included as colored circles in the top plot.

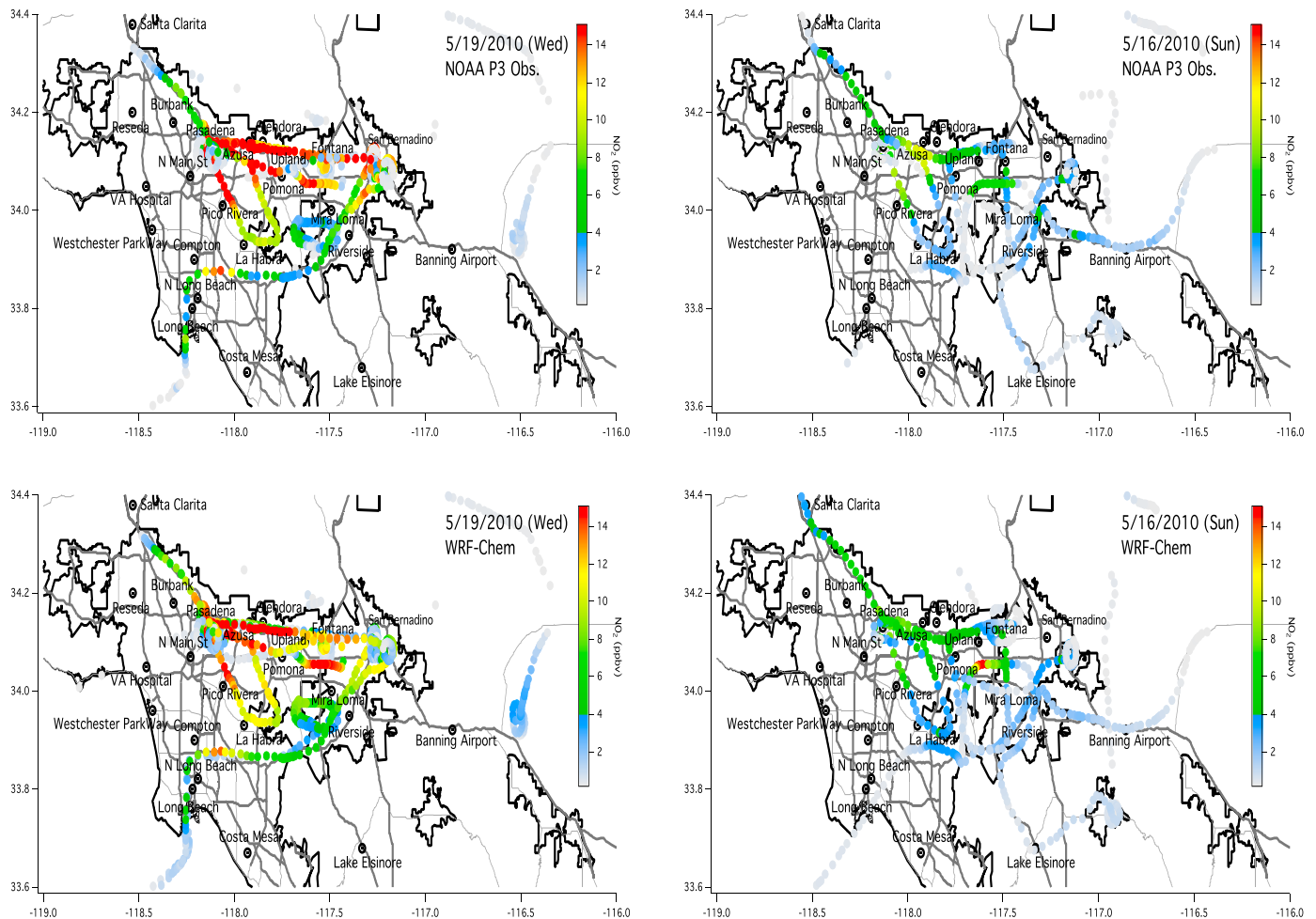


Figure 3. The NOAA P-3 aircraft-observed and the model-simulated NO₂ on a weekday (19 May 2010, left) and on a weekend (16 May 2010, right) are displayed on the flight tracks. The top (bottom) plots show the observations (model simulations). NO₂ > 0.2 ppbv is shown. The multiple observations within one model grid are averaged. A linear fit of the model simulations versus the observations has a slope = 0.72 (0.95) and a correlation coefficient = 0.87 (0.84) on 19 May 2010 (16 May 2010).

distribution of the PBL height. Therefore, it is important to validate the accuracy of the modeled vertical mixing at various locations in the basin. In Figure 2, the absolute magnitudes and shapes of vertical profiles in the simulated air temperature and water vapor agree with those in the P-3 observations, from a stable regime in Catalina Island to a few kilometer PBL height under a convectively unstable condition in Yucca Valley. Consequently, the vertical profiles of the simulated NO_x and CO match the P-3 profiles (Figure 2).

Figure 3 exemplifies the P-3 flight paths and the in situ NO₂ measurements on a weekday and weekend. The P-3 observed much lower NO₂ levels on the weekend compared to the weekday flight. The model simulated NO₂ using the emission inventory in this study reproduces the spatial and temporal distribution of observed NO₂ qualitatively in Figure 1. Averages of the P-3 NO₂, NO, NO_x, and CO and the WRF-Chem simulations representing boundary layer conditions are shown in Figure 4 and Table 5, demonstrating good agreement between the measurements and the simulations for both weekdays and weekends. On weekdays, both the observed and simulated NO_x are 11.2 ppbv on average and the correlation coefficient of the linear fit of the model results to the observations is 0.67. Both the P-3 observations and the model results indicate substantial NO_x reductions on weekends compared to weekdays. The observed NO_x on weekends is 2.9 ppbv on average, and the simulated NO_x is 3.9 ppbv with a correlation coefficient of 0.68. The weekend to weekday ratio in the simulated NO_x is 35%, while that in the observations is 26%. The weekend to weekday ratio in the simulated NO_y (=NO_x + PAN + HNO₃) is 50%, while that in the observations is 49%. *Valin et al., 2014* suggested that the ambient level of NO₂ on weekends is affected by enhanced photochemistry as well as the emission changes.

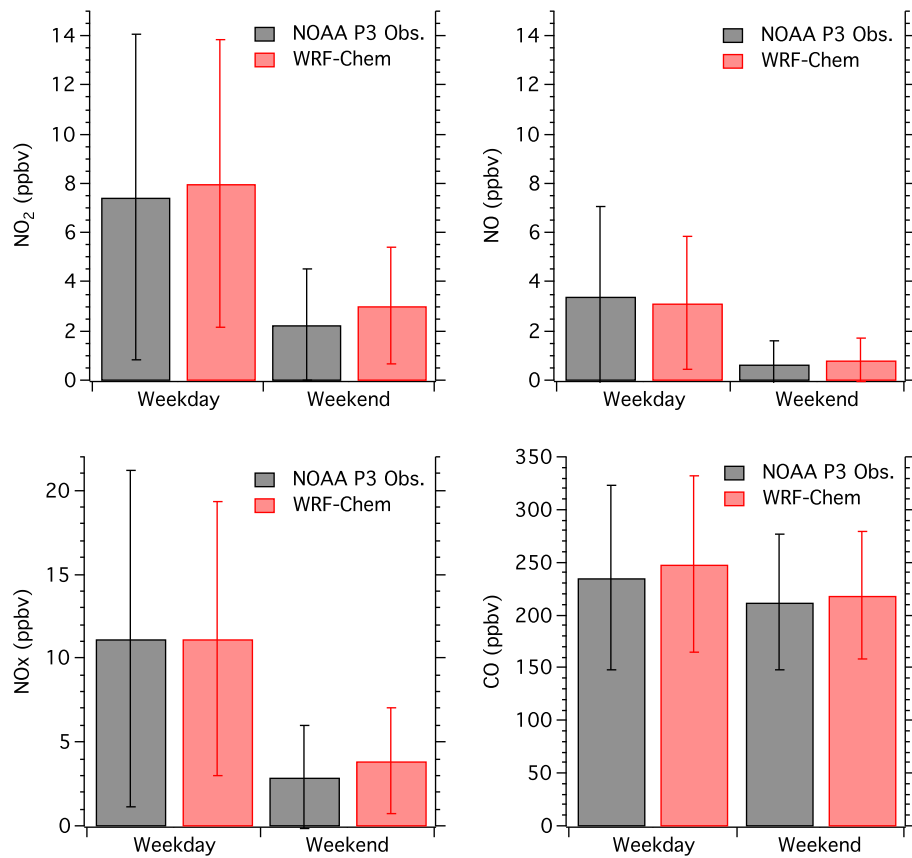


Figure 4. The P-3 aircraft observations (black bars) of NO_2 , NO , NO_x , and CO and the corresponding model simulations (red bars) averaged over the SoCAB (33.55°N – 34.55°N , 118.60°W – 116.60°W) for weekdays and weekends. The model output along the flight tracks is included. The standard deviations are shown as vertical thin lines.

In contrast to NO_x , both the P-3 observed CO and the simulations do not show a distinct weekly cycle. The weekend to weekday ratio in the observations is 90%, while that in the simulations is 88% for CO . Differences between the observed and the modeled CO are less than 5%.

The ratio of NO_x to CO can be a useful parameter to validate an emission inventory and identify the chemical regime relevant to tropospheric O_3 formation. The slope of the NO_x to CO correlation in Figure 5 provides a measure of the NO_x to CO enhancement ratio in the observations and the simulations. The observed ratios on weekdays and weekends are 0.11 and 0.033, respectively. The simulated ratios on weekdays and weekends are 0.088 and 0.035, respectively, which are close to the observed ratios. Reduced diesel vehicle activities decrease the enhancement ratio on weekends. The correlation coefficient of the linear fit of NO_x to CO is

Table 5. Comparison of NOAA-P-3 Observations and WRF-Chem Simulations Averaged Over the SoCAB (33.55°N – 34.55°N , 118.60°W – 116.60°W)^a

Spec.	Weekdays			Weekends		
	Observation Mean (SD) ^b	Model Mean (SD)	Corr. Coef.	Observation Mean (SD)	Model Mean (SD)	Corr. Coef.
NO_x	11.2 (10.0)	11.2 (8.2)	0.67	2.9 (3.0)	3.9 (3.1)	0.68
NO_2	7.5 (6.6)	8.0 (5.8)	0.67	2.3 (2.2)	3.0 (2.4)	0.70
NO	3.4 (3.7)	3.1 (2.7)	0.66	0.7 (0.9)	0.9 (0.9)	0.61
CO	235.3 (87.1)	248.2 (83.5)	0.64	212.3 (64.2)	219.2 (60.9)	0.72
O_3	56.7 (12.4)	52.3 (13.7)	0.75	72.2 (11.8)	65.2 (17.3)	0.61
O_x	63.7 (11.4)	59.8 (15.3)	0.79	74.5 (11.8)	68.1 (17.8)	0.64

^aMean and standard deviation are in ppbv.

^bStandard deviation.

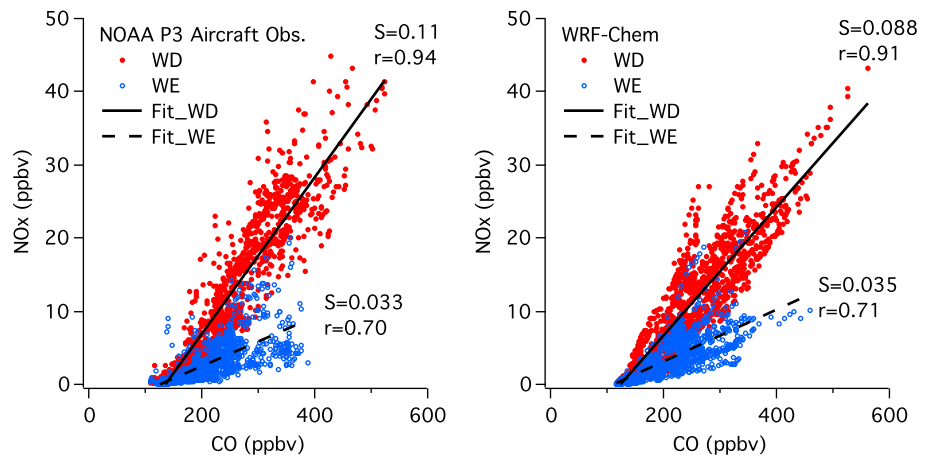


Figure 5. Comparison of the weekday (WD, red filled circles) and the weekend (WE, blue open circles) NO_x to CO ratios from (left) the P-3 aircraft observations and (right) the WRF-Chem model simulations in the SoCAB (33.55°N–34.55°N, 118.60°W–116.60°W). The linear fits for weekdays and weekends are shown as solid and dashed lines, respectively. The slopes (S) and correlation coefficients (r) from the fits are included in the plots.

~0.9 on weekdays and is ~0.7 on weekends, seen in both the observations and simulations. The similar results using NO_y (=NO_x + PAN + HNO₃) and CO are shown in Figure S12.

5.2.2. Ground-Based Observations of NO₂ and CO in Pasadena

Ground-based in situ observations of NO₂ and CO in Pasadena were sampled on more days (mid-May to mid-June) than the aircraft observations and provide another measure of the performance of the emission inventory. Figure 6 illustrates diurnal variations of ground-based NO₂ and CO and the corresponding model simulations, which show peaks near noon due to the local emissions and transport of pollutants from west of Pasadena including Downtown LA, as in Figure 1. On average, the model simulated NO₂ agrees with the measurements by NOAA CRDS and University of Colorado CE-DOAS, reproducing the weekday-weekend contrast of NO₂. The model NO₂ is only 9–14% higher than the observations on average. The weekend to weekday ratio in the observed NO₂ is 53%–61%, depending on the instruments, and the model ratio agrees with the observed ratio. Modeled NO₂ is overestimated compared to the observations during morning hours until noon. Disagreement in this time period is examined further with AMAX-DOAS and ground-based MAX-DOAS data and the model results in section 5.3. The modeled CO agrees with observations in both the daytime averages and diurnal profiles. The simulated CO is only 1% lower than the observations.

5.3. Comparison of CalNex Remote Sensing NO₂ Observations and Model Results

5.3.1. Airborne MAX-DOAS NO₂ Columns Over the SoCAB

The NOAA Twin-Otter aircraft made measurements in the western and eastern portions of the SoCAB, extending from morning to afternoon hours. Figure 7 highlights the flight paths and AMAX-DOAS NO₂ columns on a weekday and weekend. The AMAX-DOAS recorded decreased NO₂ on the weekend compared to the weekday for a north-south flight segment from Long Beach to Pasadena following Highway 710. Generally, the model simulated NO₂ using the emission inventory developed in this study reproduced the spatial and temporal distribution of the observed NO₂. The model overestimates NO₂ columns for several flight segments for both the weekday and the weekend.

The averages of AMAX-DOAS NO₂ and the WRF-Chem simulations are shown in Figure 8 and Table 6. Figure 8 shows reasonable agreement between the observed NO₂ columns and the model results for both weekdays and weekends, with the model NO₂ being 27% (50%) higher than the observations on weekdays (weekends). On weekdays, the observed NO₂ column is 11.2×10^{15} molecules cm⁻² on average and the simulated NO₂ is 14.2×10^{15} molecules cm⁻² with a correlation coefficient of 0.63. The observed NO₂ column on weekends is 7.7×10^{15} molecules cm⁻² on average, and the simulated NO₂ is 11.5×10^{15} molecules cm⁻² with a correlation coefficient of 0.62. The weekend to weekday ratio in the observed (simulated) NO₂ is 69% (81%). The location and time of AMAX-DOAS measurements used in this study may affect the weekend to weekday ratio. The weekdays are Monday and Friday, and the weekends in this analysis include the Independence Day

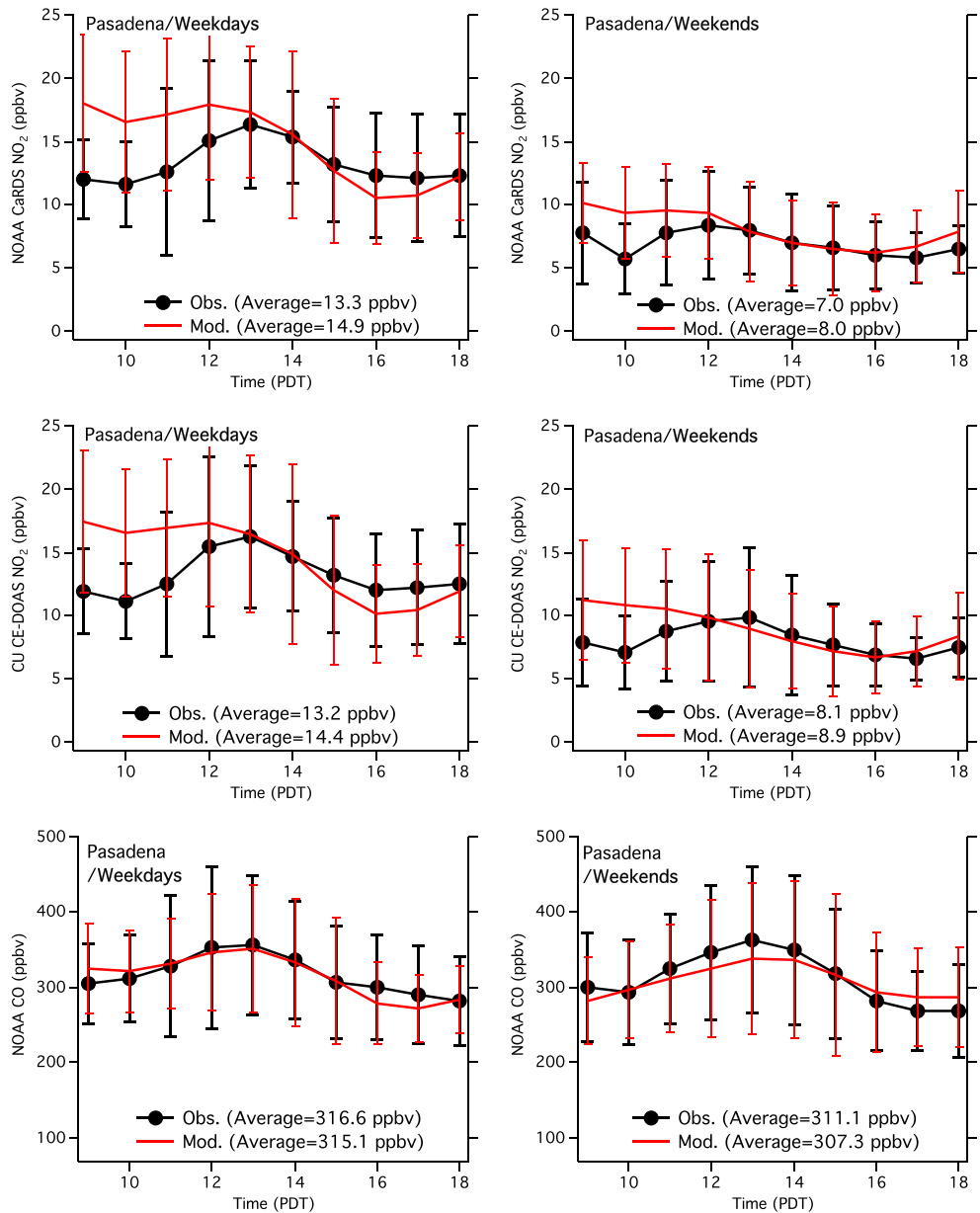


Figure 6. Diurnal variations of ground-based observations (black filled circles with solid lines) of NO₂ and CO and the corresponding model simulations (red solid lines) in Pasadena (34.1370°N, 118.1254°W) averaged for (left) weekdays and (right) weekends. The standard deviations are shown as vertical lines.

National Holiday (Monday 5 July 2010). The data under solar zenith angle <30° cover morning to early afternoon. We utilize average diurnal and day-of-week profiles that may not reflect emissions on national holidays. The higher model than observed ratio may be due in part to adopting Sunday emissions for the Independence Day, causing smaller modulation in NO₂ columns in the model than the observations. The AMAX-DOAS and OMI data sets both showed a reduction of NO₂ tropospheric columns on weekends by ~38% and ~33%, respectively, in the SoCAB during CalNex [Oetjen et al., 2013] utilizing all available AMAX-DOAS data.

Positive biases in the model NO₂ relative to AMAX-DOAS data may indicate uncertainties in the spatial and temporal patterns of our emission inventory. This suggests that fine-resolution NO₂ column observations at various times of day, similar to the AMAX-DOAS data, are useful to constrain NO_x emissions. Baidar et al. [2013b] have used the AMAX-DOAS data to map and quantify the NO_x emissions in the

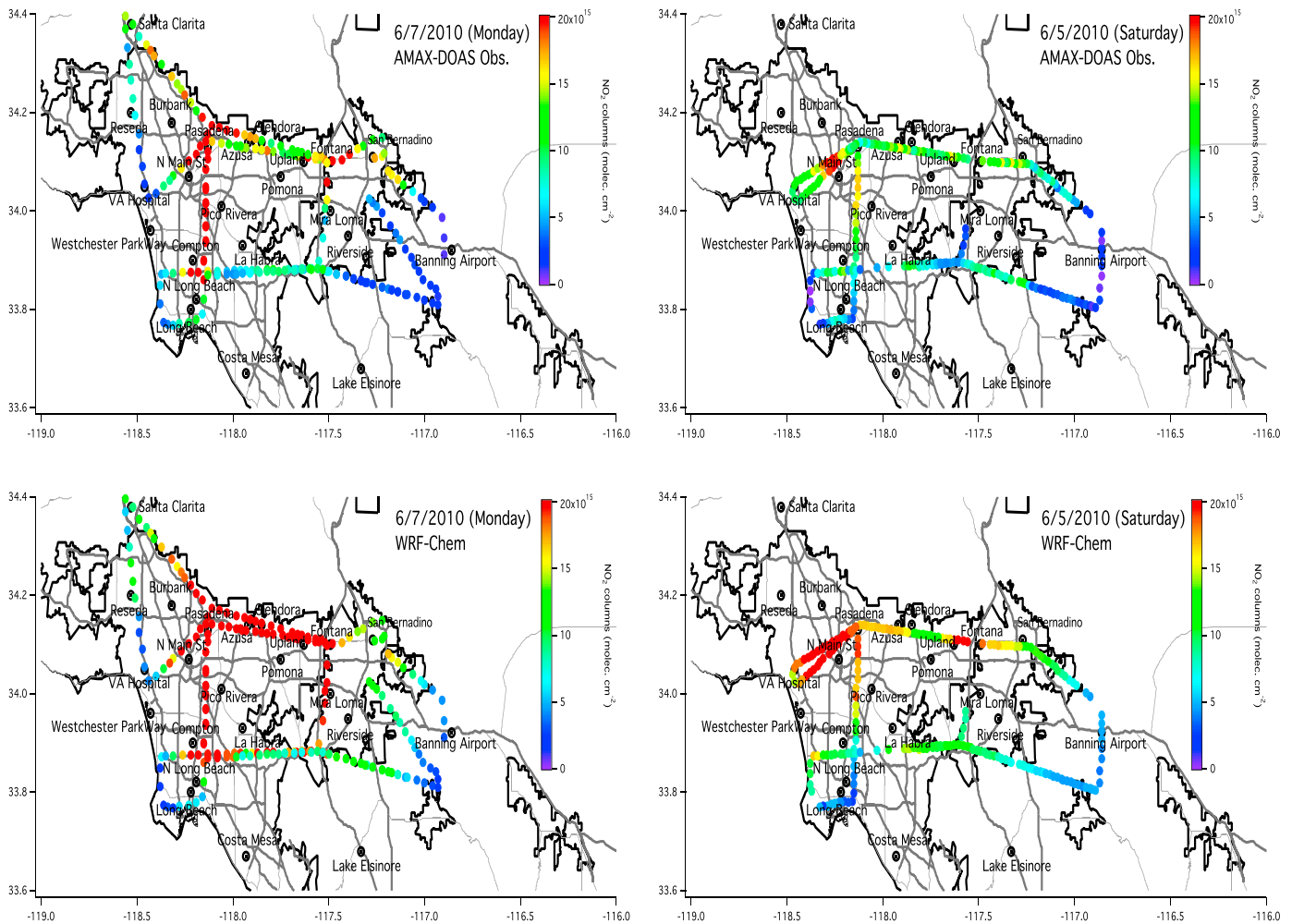


Figure 7. The NOAA Twin-Otter Airborne MAX-DOAS and the model-simulated NO_2 columns on a weekday (7/June/2010, left) and on a weekend (5/June/2010, right) are displayed on the flight tracks. The top (bottom) plots show the observations (model simulations). The multiple observations within one model grid are averaged. A linear fit of the model simulations versus the observations has a slope = 1.3 (0.91) and a correlation coefficient = 0.76 (0.77) on 7/June/2010 (5/June/2010).

San Joaquin Valley and found overall good agreement between their estimates and CARB 2010 emission inventory over Bakersfield city and underestimation of NO_x emissions in the bottom-up emission inventory upwind of the city. Geostationary satellite observations of NO_2 and other chemical species columns as exemplified in Figure 1 will provide enhanced spatial and temporal coverage for determining sectorial emissions and diurnal profiles. The Tropospheric Emissions: Monitoring of Pollution (TEMPO) (<https://www.cfa.harvard.edu/atmosphere/publications/TEMPO-EO-2013.pdf>; Fishman *et al.*, 2012) instrument on board a geostationary satellite platform, which is planned to be launched in 2019–2021, will be helpful for the study of emissions, transport, and chemistry in North America.

5.3.2. Ground-Based MAX-DOAS NO_2 Columns in Pasadena

During CalNex, the ground-based remote sensing measurements of NO_2 columns in Pasadena were collected on more days (1 May to 18 July) than the airborne remote sensing observations. Figure 9 provides diurnal variations of ground-based NO_2 columns and the corresponding model simulations on weekdays and weekends. On average, the model simulated NO_2 is 12–15% higher than the retrieved NO_2 columns. The model reproduces the weekday-weekend contrast of NO_2 columns in Pasadena. The weekend to weekday ratios in both the observed and simulated NO_2 are 58–60%. There is a slight overestimation of the model NO_2 compared to the retrieval between morning and noon as found in in situ data and the model at this location. Overall, in Pasadena, the model bias to the remote sensing NO_2 observations is consistent with the model bias to in situ measurement data (see section 5.2).

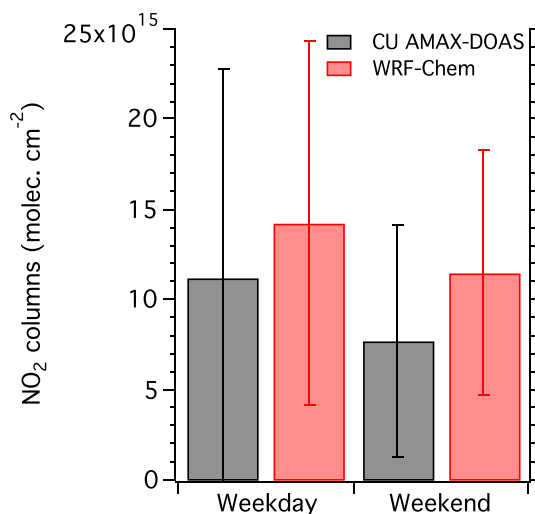


Figure 8. The Twin-Otter Airborne MAX-DOAS observed (black bars) and the model simulated (red bars) NO₂ columns averaged over the SoCAB (33.55°N–34.55°N, 118.60°W–116.60°W) for weekdays and weekends. For comparison of weekdays and weekends, the data from ~11:00 PDT to ~14:00 PDT are shown. The standard deviations are shown as vertical thin lines.

5.4. Comparison of the AQMD In Situ NO_x and CO Observations and Model Results

We also utilized the AQMD surface monitor NO_x and CO at 21 stations for validation of the emissions of NO_x and CO. In Figure 10, the diurnal cycles of the model simulated NO_x and CO across the SoCAB are compared with observations on weekdays and weekends. On average, the model simulated NO_x and CO resemble strikingly the AQMD observations. The peaks of the observations occur at 06:00–07:00 PDT, and those of the simulations are found at the same time or with an hour delay. The minimum occurs at 16:00 PDT in both the observations and model simulations. For NO_x, the weekend-to-weekday ratios in the AQMD data and corresponding model results are 56% and 52%, respectively, for the same time window (09:00 PDT–18:00 PDT) used for the CalNex in situ and remote sensing NO₂ data in Pasadena. For CO, an 8% and 6% reduction on weekends is found in the measurements and model results, respectively.

In spite of agreement in the averages, the standard deviation of the simulated NO_x is underestimated in the early morning and late afternoon and that of the simulated CO is underestimated throughout the day. An examination of data from individual stations indicates that the model overestimates NO_x at several sites located south and west of Pasadena (e.g., Los Angeles International Airport (LAX), Long Beach) and underestimates NO_x at sites located east of Pasadena (e.g., Pomona, Fontana) in the morning. These errors cancel during averaging and may cause the discrepancy in the standard deviations in the early morning (Figures S10 and S11 and Table S6). In the afternoon, the AQMD NO_x measurements may include other reactive nitrogen species such as PAN, HNO₃, and organic nitrates [Fehsenfeld et al., 1987; Dunlea et al., 2007], which may cause larger averages and standard deviations in the observations than the simulations at this time. Model NO_x overestimates at the AQMD sites located in Pasadena and south and west of Pasadena during the night and in to the morning confirm the findings from the comparison of the model NO₂ with the CalNex AMAX-DOAS and in situ and remote sensing NO₂ in Pasadena, indicating room for improvement in the spatial and temporal representation of the emission inventory. For example, spatial and temporal distributions from NEI05 for nonroad mobile and areawide and stationary sources were used in this study, which may cause errors in the NO_x emission estimations from these sources. In addition, pollution control measures on locomotive engines (<http://www.arb.ca.gov/railyard/railyard.htm>) and other stationary sources, and their impacts need to be tracked carefully. Real-time traffic data sets could also help with improving on-road emission patterns. The observed CO shows larger variability than the simulation. This may indicate that the emission inventory underestimates the variability in CO emissions. Furthermore,

Table 6. Comparison of CU AMAX-DOAS NO₂ Columns Observations (From ~11:00 PDT to 14:00 PDT) and WRF-Chem Simulations Averaged Over the SoCAB (33.55°N–34.55°N, 118.60°W–116.60°W)^a

Period	Observation Mean (SD ^b)	Model Mean (SD)	Correlation Coefficient
All days	9.38 × 10 ¹⁵ (9.39 × 10 ¹⁵)	12.82 × 10 ¹⁵ (8.65 × 10 ¹⁵)	0.63
Weekdays	11.20 × 10 ¹⁵ (11.54 × 10 ¹⁵)	14.23 × 10 ¹⁵ (10.11 × 10 ¹⁵)	0.63
Weekends	7.71 × 10 ¹⁵ (6.44 × 10 ¹⁵)	11.53 × 10 ¹⁵ (6.81 × 10 ¹⁵)	0.62

^aMean and standard deviation are in molecules cm⁻².
^bStandard deviation.

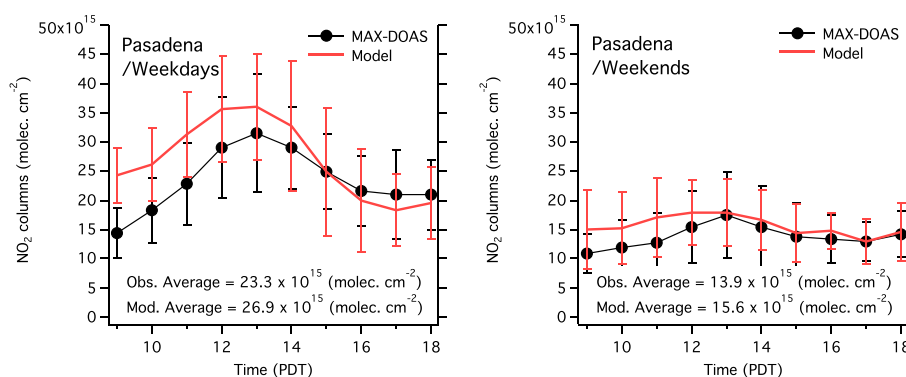


Figure 9. Diurnal variation of ground-based MAX-DOAS NO_2 columns (circles with black solid lines) and the model simulations (red solid lines) in Pasadena (34.1370°N , 118.1254°W) averaged for (left) weekdays and (right) weekends. The standard deviations of the MAX-DOAS observations and model simulations are shown as vertical lines.

the model horizontal and vertical resolutions may not be enough to capture the spatial gradient of NO_x and CO near roadside monitors. In addition, uncertainties in the model representations of PBL and chemistry during night and morning transition time are not well understood. If the model PBL is underestimated at these times, the simulated NO_x and CO mixing ratios can be overestimated. Research for better understanding of nighttime chemistry that might affect NO_x budget has been conducted [Stutz *et al.*, 2004; Brown *et al.*, 2007; Young *et al.*, 2012; VandenBoer *et al.*, 2013]. Future studies will need to include sensitivities of the model NO_x to various assumptions of nighttime chemistry.

Figure 10 also includes the measured and simulated O_3 at the surface monitors averaged for weekdays and weekends. It exhibits higher O_3 on the weekends in both the observations and the model results, as demonstrated in the previous studies [e.g., Fujita *et al.*, 2003; Harley *et al.*, 2005; Pollack *et al.*, 2012]. More detailed analysis of weekend O_3 is summarized in next section, using P-3 data and model simulations.

5.5. Weekend Effect on O_3

Evidence of faster photochemistry on weekends during CalNex, such as higher O_3 , O_x , PAN, and HCHO on weekends compared to weekdays, was reported by Pollack *et al.* [2012] and Warneke *et al.* [2013] based on NOAA P-3 and surface measurements. While higher surface O_3 on weekends remains widespread, a recent analysis of AMAX-DOAS and lidar observations on the NOAA Twin Otter and long-term ground measurements shows that the spatial extent and the trend in the probability of weekend O_3 effect occurrences have decreased significantly compared to a decade ago [Baidar *et al.*, 2015]. In this section, with the new emission inventory, the model's skill in reproducing NOAA P-3 O_3 and related tracers and their modulations between weekday and weekend is examined. Figure 11 shows that the P-3 and the model O_3 agree reasonably well (4–7 ppbv absolute model bias) and both have higher O_3 and O_x on weekends. Table 5 summarizes the statistics of O_3 and O_x . On weekdays, on average, the P-3 and the model O_3 are 56.7 and 52.3 ppbv, respectively. Weekend O_3 (O_x) is increased by 15.5 (10.7) and 12.9 (8.3) ppbv in the observations and the simulations, respectively, compared to weekday O_3 (O_x). VOC is also important to simulate O_3 and related tracers. As suggested in Borbon *et al.* [2013], NEI05 VOC emissions need to be improved. Despite limitations in the representation of VOC emissions, it was still possible to simulate the weekend O_3 effects using the NO_x and CO emissions implemented in this study.

The observed increase in PAN on weekends highlights a significant enhancement in photochemistry [Pollack *et al.*, 2012]. The weekday and weekend PAN measured from the P-3 are 0.62 and 1.03 ppbv, respectively, while the weekday and weekend HNO_3 were 3.03 and 2.59 ppbv, respectively. Therefore, the ratios of the observed PAN average to the HNO_3 average on the weekdays and weekends are 0.20 and 0.40, respectively. The increase of PAN/ HNO_3 on weekends suggests enhanced ozone production efficiency [e.g., Jacob, 1999] due to lower NO_x . The simulated PAN averages on the weekdays and weekends are 0.75 and 1.14 ppbv, respectively, while the simulated HNO_3 averages on weekdays and weekends are 3.89 and 2.78 ppbv, respectively. The ratios of the simulated PAN average to the HNO_3 average (0.19 on weekdays and 0.41 on weekends) agree with the

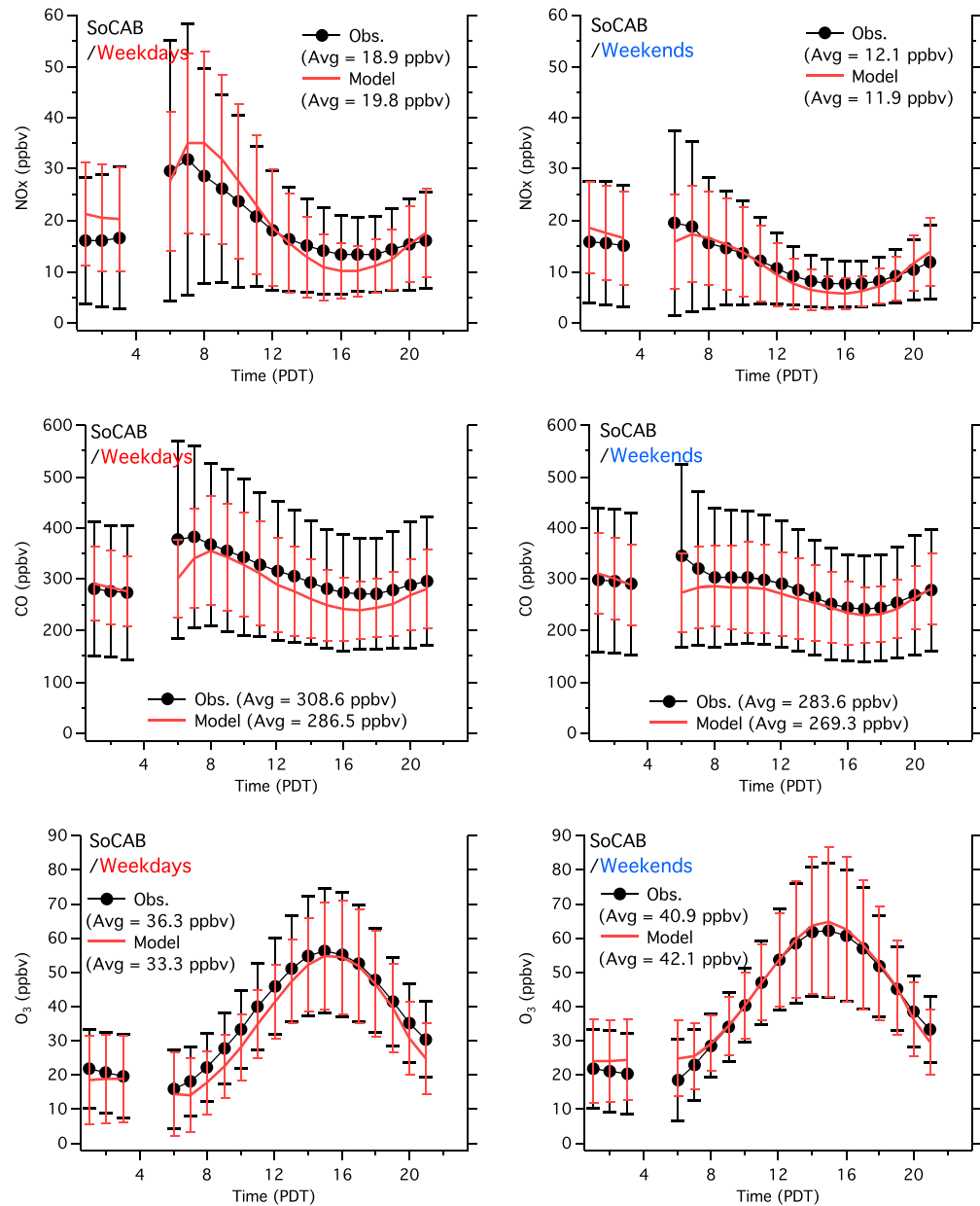


Figure 10. Diurnal variation of the 21-site-average AQMD surface measurements (black filled circles with solid lines) of NO_x, CO, and O₃ and the corresponding model simulations (red solid lines) over the SoCAB averaged for (left) weekdays and (right) weekends. The standard deviations are shown as vertical lines.

observations. The simulated PAN and HNO₃ mixing ratios are 7%–28% higher than the observations probably due to limitations in the VOC emissions used in the model or uncertainties in the measurements. Similar results based on the linear regression fits are shown in Figure S13.

The weekday-to-weekend differences in PAN to CO ratio (PAN/CO) and O_x to CO ratio (O_x/CO), derived from slopes of the correlations of these species, are examined in Figure 12. These weekday-to-weekend differences can be used as parameters for validating the model's urban photochemistry and consequently its emission inventory. The aircraft observed PAN to CO ratio on weekends is 0.008, 4 times higher than the value on weekdays (0.002), which again substantiates enhanced photochemistry on weekends. The model also simulates increased PAN/CO on weekends compared to weekdays, although the simulated PAN/CO is higher than the observed ratio, especially on weekdays. The correlation between the simulated PAN and CO is higher

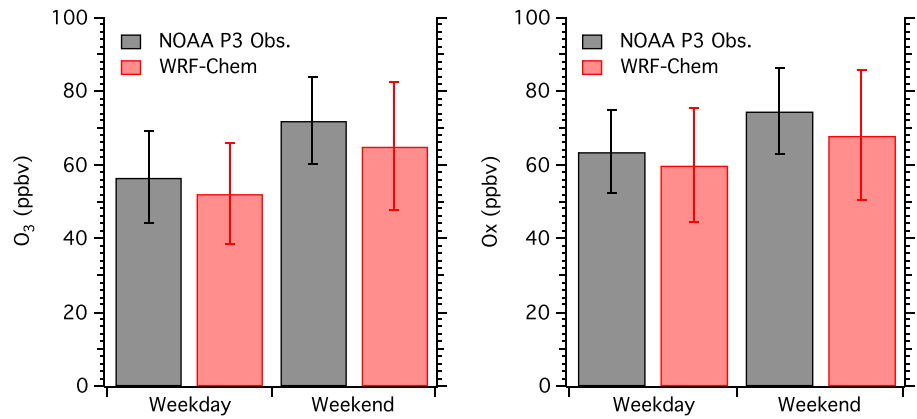


Figure 11. The P-3 aircraft observations (black bars) of (left) O₃ and (right) O_x and the corresponding model simulations (red bars) averaged over the SoCAB (33.55°N–34.55°N, 118.60°W–116.60°W) for weekdays and weekends. The standard deviations are shown as vertical thin lines.

than that between the observed mixing ratios of these species. Both the observed and simulated O_x/CO on weekends is higher than the ratio on weekdays. The correlation between the simulated O_x and CO is higher than that for the corresponding observations. The O_x intercept from a linear fit of observed O_x to CO is higher than that in the simulations, but the observed slope is lower than the simulations. This may indicate

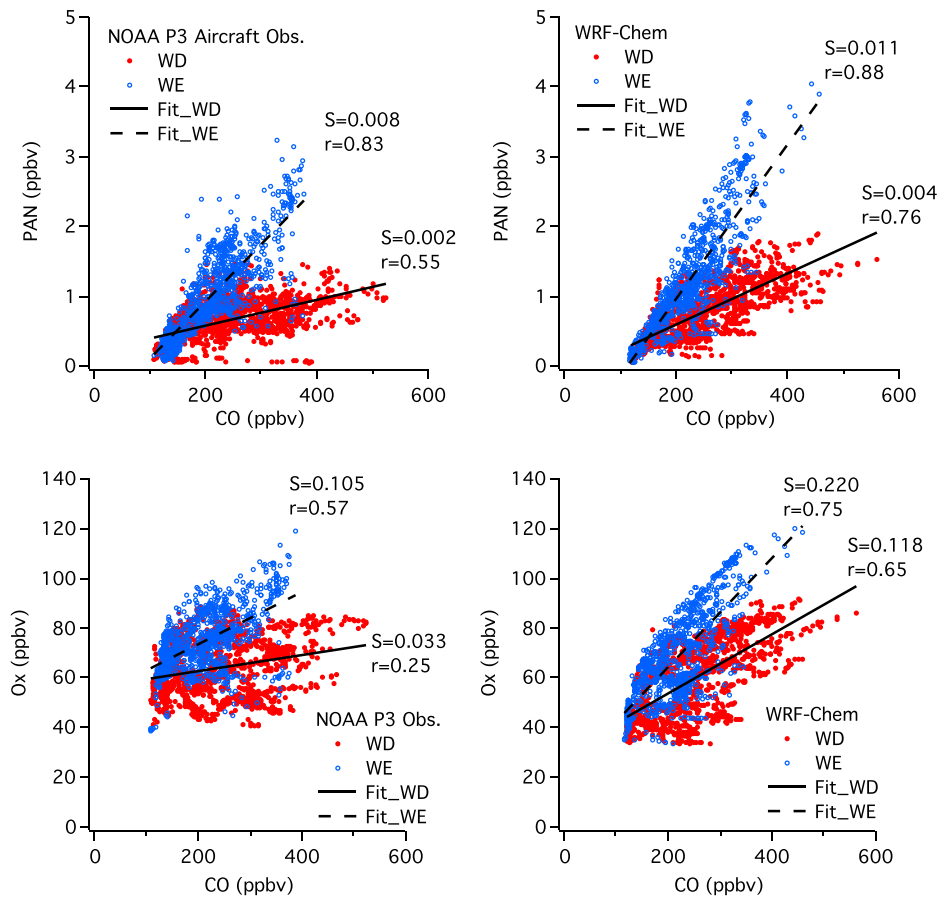


Figure 12. Comparison of the weekday (WD, red filled circles) and the weekend (WE, blue open circles) PAN to CO ratios from (left) the P-3 aircraft observations and (right) the WRF-Chem model simulations in the SoCAB (33.55°N–34.55°N, 118.60°W–116.60°W). The ratios of O_x to CO are also shown. The linear fits for weekdays and weekends are shown as solid and dashed lines, respectively. The slopes (S) and correlation coefficients (r) from the fits are included in the plots.

limitations in the model background O₃, plume chemistry, and VOC emission inventory. We are developing a VOC inventory for CalNex and California and plan to revisit this issue with model simulations using the new VOC inventory.

6. Summary and Conclusions

We have developed a new bottom-up NO_x and CO emissions inventory utilizing an expanded version of the Fuel-based Inventory for Vehicle Emissions [McDonald *et al.*, 2012, 2013, 2014] for modeling air quality during CalNex. Fuel sales data and measured emission factors for gasoline and diesel powered motor vehicles are utilized to calculate total on-road mobile source emissions. These emissions are spatially and temporally allocated using traffic count data. For other sectors, either a fuel-based approach or the emission estimates in CARB 2009 Almanac-Standard Emissions Tool are adopted and are temporally and spatially distributed following the U.S. EPA's NEI05 inventory. In addition to NO_x and CO, VOC emissions are required for model simulations. We use the NEI05 VOC to generate model outputs to validate the NO_x and CO inventory and to investigate O₃ formation chemistry.

Overall, the model simulations utilizing the NO_x and CO emission inventory developed in this study agree with in situ and remote sensing airborne and surface observations in the SoCAB. Weekday-to-weekend changes in NO_x and CO measured during CalNex are well reproduced using the emission inventory developed for this study: a substantial reduction in NO_x on weekends and little daily change in CO. Even with the NEI05-derived representation of VOC emissions used here, the model simulates changes in the photochemistry observed on weekends. Both the observations and the model results demonstrate higher O₃, O_x, and PAN on weekends than on weekdays, showing the importance of local NO_x and VOC chemistry in this region.

Our assessment indicates that the spatial and temporal patterns in the inventory developed in this study can be improved. The inventory can be refined by using the spatial and temporal distributions of an updated CARB emission inventory and NEI11 for other mobile and stationary sources (e.g., offroad equipment, commercial marine vessels, and point sources). For on-road emissions, incorporating real-time traffic data sets may help with improving the emission patterns.

The regional chemical transport model used in this study played an important role in connecting the surface emissions to ambient observations obtained from multiple platforms. However, incomplete measurement coverage as well as uncertainties in the model's mixing and transport may limit full understanding of emissions and chemistry in the SoCAB. This study suggests that the chemical measurements from geostationary satellites could provide powerful constraints on the spatial and temporal distribution of the emissions and their impacts when those remote sensing data are well calibrated and validated.

This study builds a foundation to construct a long-term record of changes in NO_x and CO emissions and to understand the contributors to long-term O₃ changes in California. By utilizing global model results as a boundary condition, future research using a regional model to study the O₃ trend may also consider the impacts of Asian emission changes and stratosphere-troposphere exchange on California background O₃.

References

- Ahmadov, R., *et al.* (2015), Understanding high wintertime ozone pollution events in an oil- and natural gas-producing region of the western US, *Atmos. Chem. Phys.*, *15*, 411–429, doi:10.5194/acp-15-411-2015.
- Alvarez, R. J., *et al.* (2011), Development and application of a compact, tunable, solid-state airborne ozone lidar system for boundary layer profiling, *J. Atmos. Oceanic Technol.*, *28*, 1258–1272, doi:10.1175/JTECH-D-10-05044.1.
- Anderson, D. C., *et al.* (2014), Measured and modeled CO and NO_y in DISCOVER-AQ: An evaluation of emissions and chemistry over the eastern US, *Atmos. Environ.*, *96*, 78–87, doi:10.1016/j.atmosenv.2014.07.004.
- Angevine, W. M., L. Eddington, K. Durkee, C. Fairall, L. Bianco, and J. Brioude (2012), Meteorological model evaluation for CalNex, *Mon. Weather Rev.*, *140*, 3885–3906, doi:10.1175/MWR-D-12-00042.1.
- Baidar, S., H. Oetjen, S. Coburn, B. Dix, I. Ortega, R. Sinreich, and R. Volkamer (2013a), The CU Airborne MAX-DOAS instrument: vertical profiling of aerosol extinction and trace gases, *Atmos. Meas. Tech.*, *6*, 719–739, doi:10.5194/amt-6-719-2013.
- Baidar, S., R. Volkamer, R. Alvarez, A. Brewer, F. Davies, A. Langford, H. Oetjen, G. Pearson, C. Senff, and R. M. Hardesty (2013b), Combining active and passive airborne remote sensing to quantify NO₂ and O_x production near Bakersfield, CA, 2013, *Br. J. Environ. Clim. Change*, *3*(4), 566–586, doi:10.9734/BJECC/2013/5740.
- Baidar, S., R. M. Hardesty, S.-W. Kim, A. O. Langford, H. Oetjen, C. Senff, M. Trainer, and R. Volkamer (2015), Weakening of the weekend ozone effect over California's South Coast Air Basin, *Geophys. Res. Lett.*, *42*, 9457–9464, doi:10.1002/2015GL066419.

Acknowledgments

The first author thanks Jerome Brioude, Yuyan Cui, Ravan Ahmadov, Sang-Hyun Lee, Wayne Angevine, Eric Williams, Jim Kelly, Chenxia Cai, Ajith Kaduwela, and Andreas Richter for the discussions and assistance. R. Volkamer acknowledges funding from NSF-CAREER award ATM-847793, and California Air Resources Board contract ARB 09-317. S. Baidar is a recipient of the CIRES-ESRL graduate fellowship. The NOAA Health of Atmosphere program, the NASA ROSES ACPMAP (NNH14AX011), and NASA GEO-CAPE Mission Pre-formulation Study (NNH13AW311) supported this research. The WRF-Chem model version 3.4.1 used in this study is available at http://www2.mmm.ucar.edu/wrf/users/download/get_source.html. We acknowledge the use of MOZART-4 global model output available at <http://www.aocom.ucar.edu/wrf-chem/mozart.shtml>. The CalNex field campaign data are available at <http://www.esrl.noaa.gov/csd/projects/calnex/>.

- Ban-Weiss, G. A., J. P. McLaughlin, R. A. Harley, M. M. Lunden, T. W. Kirchstetter, A. J. Kean, A. W. Strawa, E. D. Stevenson, and G. R. Kendall (2008a), Long-term changes in emission of nitrogen oxides and particulate matter from on-road gasoline and diesel vehicles, *Atmos. Environ.*, *42*, doi:10.1016/j.atmosenv.2007.09.049.
- Ban-Weiss, G. A., J. McLaughlin, R. A. Harley, A. Kean, E. Grosjean, and D. Grosjean (2008b), Carbonyl and nitrogen dioxide emissions from gasoline- and diesel-powered motor vehicles, *Environ. Sci. Technol.*, *42*(11), 3944–3950.
- Bishop, G. A., and D. H. Stedman (2008), A decade of on-road emissions measurements, *Environ. Sci. Technol.*, *42*, 1651–1656, doi:10.1021/es702413b.
- Borbon, A., et al. (2013), Emission ratios of anthropogenic volatile organic compounds in northern mid-latitude megacities: Observations versus emission inventories in Los Angeles and Paris, *J. Geophys. Res. Atmos.*, *118*, 2041–2057, doi:10.1002/jgrd.50059.
- Brioude, J., et al. (2013), Top-down estimate of surface flux in the Los Angeles Basin using a mesoscale inverse modeling technique: Assessing anthropogenic emissions of CO, NO_x, and CO₂ and their impacts, *Atmos. Chem. Phys.*, *13*, 3661–3677, doi:10.5194/acp-13-3661-2013.
- Brown, S. S., W. P. Dube, H. D. Osthoff, D. E. Wolfe, W. M. Angevine, and A. R. Ravishankara (2007), High resolution vertical distributions of NO₃ and N₂O₅ through the nocturnal boundary layer, *Atmos. Chem. Phys.*, *7*, 139–149.
- Chen, D., et al. (2013), WRF-Chem simulation of NO_x and O₃ in the L.A. basin during CalNex-2010, *Atmos. Environ.*, *81*, 421–432.
- Chinkin, L. R., D. L. Coe, T. H. Funk, H. R. Hafner, P. T. Roberts, P. A. Ryan, and D. R. Lawson (2003), Weekday versus weekend activity patterns for ozone precursor emission in California's South Coast Air Basin, *J. Air Waste Manage.*, *53*(7), 829–843.
- Coburn, S., B. Dix, R. Sinreich, and R. Volkamer (2011), The CU ground MAX-DOAS instrument: characterization of RMS noise limitations and first measurements near Pensacola, FL of BrO, IO, and CHOCHO, *Atmos. Meas. Tech.*, *4*, 2421–2439, doi:10.5194/amt-4-2421-2011.
- Dallmann, T. R., and R. A. Harley (2010), Evaluation of mobile source emission trends in the United States, *J. Geophys. Res.*, *115*, D14305, doi:10.1029/2010JD013862.
- Deutschmann, T., et al. (2011), The Monte Carlo atmospheric radiative transfer model McArtim: Introduction and validation of Jacobians and 3D features, *J. Quant. Spectros. Radiat. Transfer*, doi:10.1016/j.jqsrt.2010.12.009.
- Dunlea, E. J., et al. (2007), Evaluation of nitrogen dioxide chemiluminescence monitors in a polluted urban environment, *Atmos. Chem. Phys.*, *7*, 2691–2704.
- Emmons, L. K., et al. (2010), Description and evaluation of the Model for Ozone and Related chemical Tracers, version 4 (MOZART-4), *Geosci. Model Dev.*, *3*, 43–67, doi:10.5194/gmd-3-43-2010.
- Energy Information Administration (EIA) (2012), Fuel oil and kerosene sales, 2010, Rep. DOE/EIA-0535(10), U.S. Dep. of Energy, Washington, D. C.
- Fehsenfeld, F. C., et al. (1987), A ground-based intercomparison of NO, NO_x, and NO_y measurement techniques, *J. Geophys. Res.*, *92*(D12), 14,710–14,722, doi:10.1029/JD092iD12p14710.
- Fishman, J., et al. (2012), The United States' Next Generation of Atmospheric Composition and Coastal Ecosystem Measurements: NASA's Geostationary Coastal and Air Pollution Events (GEO-CAPE) Mission, *Bull. Am. Meteorol. Soc.*, *93*(10), 1547–1566, doi:10.1175/bams-d-11-00201.1.
- Fujita, E. R., W. R. Stockwell, D. E. Campbell, R. E. Keislar, and D. R. Lawson (2003), Evolution of the magnitude and spatial extent of the weekend ozone effect in California's South Coast Air Basin, 1981–2000, *J. Air Waste Manage.*, *53*(7), 802–815.
- Gerbig, C., S. Schmitgen, D. Kley, A. Volz-Thomas, K. Dewey, and D. Haaks (1999), An improved fast-response vacuum-UV resonance fluorescence CO instrument, *J. Geophys. Res.*, *104*(D1), 1669–1704, doi:10.1029/1998JD100031.
- Grell, G. A., S. E. Peckham, R. Schmitz, S. A. McKeen, G. Frost, W. C. Skamarock, and B. Eder (2005), Fully coupled "online" chemistry within WRF model, *Atmos. Environ.*, *39*(37), 6957–6975, doi:10.1016/j.atmosenv.2005.04.027.
- Haagen-Smit, A. J. (1952), Chemistry and physiology of Los Angeles smog, *Ind. Eng. Chem.*, *44*(6), 1342–1346.
- Hair, J. W., C. A. Hostetler, A. L. Cook, D. B. Harper, R. A. Ferrare, T. L. Mack, W. Welch, L. R. Izquierdo, and F. E. Hovis (2008), Airborne High Spectral Resolution Lidar for profiling aerosol optical properties, *Appl. Optics*, *47*(36), 6734–6752.
- Harley, R. A., L. C. Marr, J. K. Lehner, and S. N. Giddings (2005), Changes in motor vehicle emissions on diurnal to decadal time scales and effects on atmospheric composition, *Environ. Sci. Technol.*, *39*(14), 5356–5362, doi:10.1021/es048172.
- Hilboll, A., A. Richter, and J. P. Burrows (2013), Long-term changes of tropospheric NO₂ over megacities derived from multiple satellite instruments, *Atmos. Chem. Phys.*, *13*, 4145–4169, doi:10.5194/acp-13-4145-2013.
- Holloway, J. S., R. O. Jakoubek, D. D. Parrish, C. Gerbig, A. Volz-Thomas, S. Schmitgen, A. Fried, B. Wert, B. Henry, and J. R. Drummond (2000), Airborne intercomparison of vacuum ultraviolet fluorescence and tunable diode laser absorption measurements of tropospheric carbon monoxide, *J. Geophys. Res.*, *105*(D19), 24,251–24,261, doi:10.1029/2000JD900237.
- Huang, M., K. W. Bowman, G. R. Carmichael, R. Bradley Pierce, H. M. Worden, M. Luo, O. R. Cooper, I. B. Pollack, T. B. Ryerson, and S. S. Brown (2013), Impact of Southern California anthropogenic emissions on ozone pollution in the mountain states: Model analysis and observational evidence from space, *J. Geophys. Res. Atmos.*, *118*, 12,784–12,803, doi:10.1002/2013JD020205.
- Huang, M., et al. (2014), Changes in nitrogen oxides emissions in California during 2005–2010 indicated from top-down and bottom-up emission estimates, *J. Geophys. Res. Atmos.*, *119*, 12,928–12,952, doi:10.1002/2014JD022268.
- Jacob, D. J. (1999), *Introduction to Atmospheric Chemistry*, Princeton Univ. Press, Princeton, N. J.
- Jacobson, M. Z. (2005), *Fundamentals of Atmospheric Modeling*, 2nd ed., Cambridge Univ. Press, New York.
- Jacobson, M. Z., R. Lu, R. P. Turco, and O. B. Toon (1996), Development and application of a new air pollution model system, I, Gas-phase simulations, *Atmos. Environ.*, *30B*, 1939–1963.
- Kean, A. J., R. A. Harley, and G. R. Kendall (2003), Effects of vehicle speed and engine load on motor vehicle emissions, *Environ. Sci. Technol.*, *37*, 3739–3746, doi:10.1021/es0263588.
- Kim, S.-W., A. Heckel, G. J. Frost, A. Richter, J. Gleason, J. P. Burrows, S. McKeen, E.-Y. Hsie, C. Granier, and M. Trainer (2009), NO₂ columns in the western United States observed from space and simulated by a regional chemistry model and their implications for NO_x emissions, *J. Geophys. Res.*, *114*, D11301, doi:10.1029/2008JD011343.
- Kim, S.-W., et al. (2011), Evaluations of NO_x and highly reactive VOC emission inventories in Texas and their implications for ozone plume simulations during the Texas Air Quality Study 2006, *Atmos. Chem. Phys.*, *11*, 11,361–11,386, doi:10.5194/acp-11-11361-2011.
- Langford, A. O., C. J. Senff, R. J. Alvarez, R. M. Banta, and R. M. Hardesty (2010), Long-range transport of ozone from the Los Angeles Basin: A case study, *Geophys. Res. Lett.*, *37*, L06807, doi:10.1029/2010GL042507.
- Lawson, D. R. (1990), The Southern California Air-Quality Study, *J. Air Waste Manage.*, *40*(2), 156–165.
- Lu, R., and R. P. Turco (1994), Air pollutant transport in a coastal environment. Part I: Two-dimensional simulations of sea-breeze and mountain effects, *J. Atmos. Sci.*, *51*, 2285–2308.
- Lu, R., R. P. Turco, and M. Z. Jacobson (1997), An integrated air pollution modeling system for urban and regional scales: 2. Simulations for SCAQS 1987, *J. Geophys. Res.*, *102*(D5), 6081–6098, doi:10.1029/96JD03502.
- Marr, L. C., and R. A. Harley (2002), Modeling the effect of weekday-weekend differences in motor vehicle emissions on photochemical air pollution in central California, *Environ. Sci. Technol.*, *36*, 4099–4106, doi:10.1021/es401034z.

- McDonald, B. C., T. R. Dallmann, E. W. Martin, and R. A. Harley (2012), Long-term trends in nitrogen oxide emissions from motor vehicles at national, state, and air basin scales, *J. Geophys. Res.*, *117*, D00V18, doi:10.1029/2012JD018304.
- McDonald, B. C., D. R. Gentner, A. H. Goldstein, and R. A. Harley (2013), Long-term trends in motor vehicle emissions in U.S. urban areas, *Environ. Sci. Technol.*, *47*, 10,022–10,031, doi:10.1021/es401034z.
- McDonald, B. C., Z. C. McBride, E. W. Martin, and R. A. Harley (2014), High-resolution mapping of motor vehicle carbon dioxide emissions, *J. Geophys. Res. Atmos.*, *119*, 5283–5298, doi:10.1002/2013JD021219.
- Millstein, D. E., and R. A. Harley (2009), Revised estimates of construction activity and emissions: Effects on ozone and elemental carbon concentrations in southern California, *Atmos. Environ.*, *43*, 6328–6335.
- Neuman, J. A., et al. (2002), Fast-response airborne in situ measurements of HNO₃ during the Texas 2000 Air Quality Study, *J. Geophys. Res.*, *107*(D20), 4436, doi:10.1029/2001JD001437.
- Neuman, J. A., et al. (2003), Calibration and evaluation of nitric acid and ammonia permeation tubes by UV optical absorption, *Environ. Sci. Technol.*, *37*(13), 2975–2981, doi:10.1021/es0264221.
- Oetjen, H., S. Baidar, N. A. Krotkov, L. N. Lamsal, M. Lechner, and R. Volkamer (2013), Airborne MAX-DOAS measurements over California: Testing the NASA OMI tropospheric NO₂ product, *J. Geophys. Res. Atmos.*, *118*, 7400–7413, doi:10.1002/jgrd.50550.
- Pollack, I. B., et al. (2011), Evaluation of ultraviolet light-emitting diodes for detection of atmospheric NO₂ by photolysis-chemiluminescence, *J. Atmos. Chem.*, *65*(2–3), 111–125, doi:10.1007/s10874-011-9184-3.
- Pollack, I. B., et al. (2012), Airborne and ground-based observations of a weekend effect in ozone, precursors, and oxidation products in the California South Coast Air Basin, *J. Geophys. Res.*, *117*, D00V05, doi:10.1029/2011JD016772.
- Pollack, I. B., T. B. Ryerson, M. Trainer, J. A. Neuman, J. M. Roberts, and D. D. Parrish (2013), Trends in ozone, its precursors, and related secondary oxidation products in Los Angeles, California: A synthesis of measurements from 1960 to 2010, *J. Geophys. Res. Atmos.*, *118*, 5893–5911, doi:10.1002/jgrd.50472.
- Roiger, A., H. Aufmhoff, P. Stock, F. Arnold, and H. Schlager (2011), An aircraft-borne chemical ionization-ion trap mass spectrometer (CI-TMS) for fast PAN and PPN measurements, *Atmos. Meas. Tech.*, *4*, 173–188, doi:10.5194/amt-4-173-2011.
- Russell, A. R., L. C. Valin, and R. C. Cohen (2012), Trends in OMI NO₂ observations over the United States: Effects of emission control technology and the economic recession, *Atmos. Chem. Phys.*, *12*, 12,197–12,209, doi:10.5194/acpd-12-12197-2012.
- Ryerson, T. B., L. G. Huey, K. Knapp, J. A. Neuman, D. D. Parrish, D. T. Sueper, and F. C. Fehsenfeld (1999), Design and initial characterization of an inlet for gas-phase NO_y measurements from aircraft, *J. Geophys. Res.*, *104*(D5), 5483–5492, doi:10.1029/1998JD100087.
- Ryerson, T. B., E. J. Williams, and F. C. Fehsenfeld (2000), An efficient photolysis system for fast-response NO₂ measurements, *J. Geophys. Res.*, *105*(D21), 26,447–26,461, doi:10.1029/2000JD900389.
- Ryerson, T. B., et al. (2013), The 2010 California Research at the Nexus of Air Quality and Climate Change (CalNex) field study, *J. Geophys. Res. Atmos.*, *118*, 5830–5866, doi:10.1002/jgrd.50331.
- Scarino, A. J., et al. (2014), Comparison of mixed layer heights from air borne high spectral resolution lidar, ground-based measurements, and the WRF-Chem model during CalNex and CARES, *Atmos. Chem. Phys.*, *14*, 5547–5560, doi:10.5194/acp-14-5547-2014.
- Scott, K. I., and M. T. Benjamin (2003), Development of biogenic volatile organic compounds emission inventory for the SCOS97-NARSTO domain, *Atmos. Environ.*, *37*(2), S39–S49.
- Slusher, D. L., L. G. Huey, D. J. Tanner, F. M. Flocke, and J. M. Roberts (2004), A thermal dissociation-chemical ionization mass spectrometry (TD-CIMS) technique for the simultaneous measurement of peroxyacyl nitrates and dinitrogen pentoxide, *J. Geophys. Res.*, *109*, D19315, doi:10.1029/2004JD004670.
- Stockwell, W. R., F. Kirchner, and M. Kuhn (1997), A new mechanism for regional atmospheric chemistry modeling, *J. Geophys. Res.*, *102*, 25,847–25,879, doi:10.1029/97JD00849.
- Stutz, J., B. Alicke, R. Ackermann, A. Geyer, A. White, and E. Williams (2004), Vertical profiles of NO₃, N₂O₅, O₃, and NO_x in the nocturnal boundary layer: 1. Observations during the Texas Air Quality Study 2000, *J. Geophys. Res.*, *109*, D12306, doi:10.1029/2003JD004209.
- Thalman, R., and R. Volkamer (2010), Inherent calibration of a blue LED-CE-DOAS instrument to measure iodine oxide, glyoxal, methyl glyoxal, nitrogen dioxide, water vapour and aerosol extinction in open cavity mode, *Atmos. Meas. Tech.*, *3*, 1797–1814, doi:10.5194/amt-3-1797-2010.
- US EPA, Office of Air Quality and Planning and Standards, Emissions, Monitoring and Analysis Division, Emissions Inventory Group, Research Park Triangle, NC (2008), Documentation for the 2005 Mobile National Emissions Inventory, Version 2.
- US EPA, Office of Air Quality and Planning and Standards, Emissions, Monitoring and Analysis Division, Emissions Inventory Group, Research Park Triangle, NC (2015), 2011 National Emissions Inventory, version 2 Technical Support Document.
- Valin, L. C., A. R. Russell, and R. C. Cohen (2014), Chemical feedback effects on the spatial patterns of the NO_x weekend effect: A sensitivity analysis, *Atmos. Chem. Phys.*, *14*, 1–9, doi:10.5194/acp-14-1-2014.
- VandenBoer, T. C., et al. (2013), Understanding the role of the ground surface in HONO vertical structure: High resolution vertical profiles during NACHTT-11, *J. Geophys. Res. Atmos.*, *118*, 10,155–10,171, doi:10.1002/jgrd.50721.
- Volkamer, R., et al. (2015), Aircraft measurements of BrO, IO, glyoxal, NO₂, H₂O, O₂-O₂ and aerosol extinction profiles in the tropics: Comparison with aircraft-/ship-based in situ and lidar measurements, *Atmos. Meas. Tech.*, *8*, 2121–2148, doi:10.5194/amt-8-2121-2015.
- Wagner, N. L., et al. (2011), Diode laser-based cavity ring-down instrument for NO₃, N₂O₅, NO, NO₂, and O₃ from aircraft, *Atmos. Meas. Tech.*, *4*(6), 1227–1240, doi:10.5194/amt-4-1227-2011.
- Wagner, T., A. Apituley, S. Beirle, S. Dörner, U. Friess, J. Remmers, and R. Shaiganfar (2014), Cloud detection and classification based on MAX-DOAS observations, *Atmos. Meas. Tech.*, *7*, 1289–1320, doi:10.5194/amt-7-1289-2014.
- Warneke, C., J. A. Degouw, J. S. Holloway, J. Peischl, T. B. Ryerson, E. Atlas, D. Blake, M. Trainer, and D. D. Parrish (2012), Multiyear trends in volatile organic compounds in Los Angeles, California: Five decades of decreasing emissions, *J. Geophys. Res.*, *117*, D00V17, doi:10.1029/2012JD017899.
- Warneke, C., et al. (2013), Photochemical aging of volatile organic compounds in the Los Angeles basin: Weekday-weekend effect, *J. Geophys. Res. Atmos.*, *118*, 5018–5028, doi:10.1002/jgrd.50423.
- Washenfelder, R. A., et al. (2011), The glyoxal budget and its contribution to organic aerosol for Los Angeles, California, during CalNex 2010, *J. Geophys. Res.*, *116*, D00V02, doi:10.1029/2011JD016314.
- White, W. H., E. S. Macias, D. F. Miller, D. E. Schorran, T. E. Hoffer, and D. P. Rogers (1990), Regional transport of the urban workweek: Methylchloroform cycles in the Nevada-Arizona Desert, *Geophys. Res. Lett.*, *17*, 1081–1084, doi:10.1029/GL017i008p01081.
- Yan, Y.-Y., J.-T. Lin, Y. Kuang, D. Yang, and L. Zhang (2014), Tropospheric carbon monoxide over the Pacific during HIPPO: Two-way coupled simulation of GEOS-Chem and its multiple nested models, *Atmos. Chem. Phys.*, *14*, 12,649–12,663, doi:10.5194/acp-14-12649-2014.
- Yarwood, G., J. Grant, B. Koo, and A. M. Dunker (2008), Modeling weekday to weekend changes in emissions and ozone in the Los Angeles basin for 1997 and 2010, *Atmos. Environ.*, *42*, 3765–3779.
- Young, C. J., et al. (2012), Vertically resolved measurements of nighttime radical reservoirs in Los Angeles and their contribution to the urban radical budget, *Environ. Sci. Technol.*, *46*, 10,965–10,973, doi:10.1021/es302206a.